Nucleic Acids Research, 2024, **52**, 14043–14060
https://doi.org/10.1093/nar/gkae996
Advance access publication date: 12 November 2024
Nucleic Acid Enzymes

Transfer RNA supplementation rescues HARS deficiency in a humanized yeast model of Charcot-Marie-Tooth disease

Sarah D.P. Wilhelm[1], Jenica H. Kakadia[1], Aruun Beharry[1], Rosan Kenana[1], Kyle S. Hoffman[2], Patrick O'Donoghue[1,3] and Ilka U. Heinemann[1,4,*]

[1]Department of Biochemistry, The University of Western Ontario, London, Ontario N6A 5C1, Canada
[2]Bioinformatics Solutions Inc, Waterloo, Ontario, N2L 3K8 Canada
[3]Department of Chemistry, The University of Western Ontario, London, Ontario N6A 5C1, Canada
[4]Children's Health Research Institute, London, ON, N6C 4V3 Canada
[*]To whom correspondence should be addressed. Tel: +1 519 850 2949; Email: ilka.heinemann@uwo.ca

Abstract

Aminoacyl-tRNA synthetases are indispensable enzymes in all cells, ensuring the correct pairing of amino acids to their cognate tRNAs to maintain translation fidelity. Autosomal dominant mutations V133F and Y330C in histidyl-tRNA synthetase (HARS) cause the genetic disorder Charcot-Marie-Tooth type 2W (CMT2W). Treatments are currently restricted to symptom relief, with no therapeutic available that targets the cause of disease. We previously found that histidine supplementation alleviated phenotypic defects in a humanized yeast model of CMT2W caused by HARS V155G and S356N that also unexpectedly exacerbated the phenotype of the two HARS mutants V133F and Y330C. Here, we show that V133F destabilizes recombinant HARS protein, which is rescued in the presence of $tRNA^{His}$. HARS V133F and Y330C cause mistranslation and cause changes to the proteome without activating the integrated stress response as validated by mass spectrometry and growth defects that persist with histidine supplementation. The growth defects and reduced translation fidelity caused by V133F and Y330C mutants were rescued by supplementation with human $tRNA^{His}$ in a humanized yeast model. Our results demonstrate the feasibility of cognate tRNA as a therapeutic that rescues HARS deficiency and ameliorates toxic mistranslation generated by causative alleles for CMT.

Graphical abstract

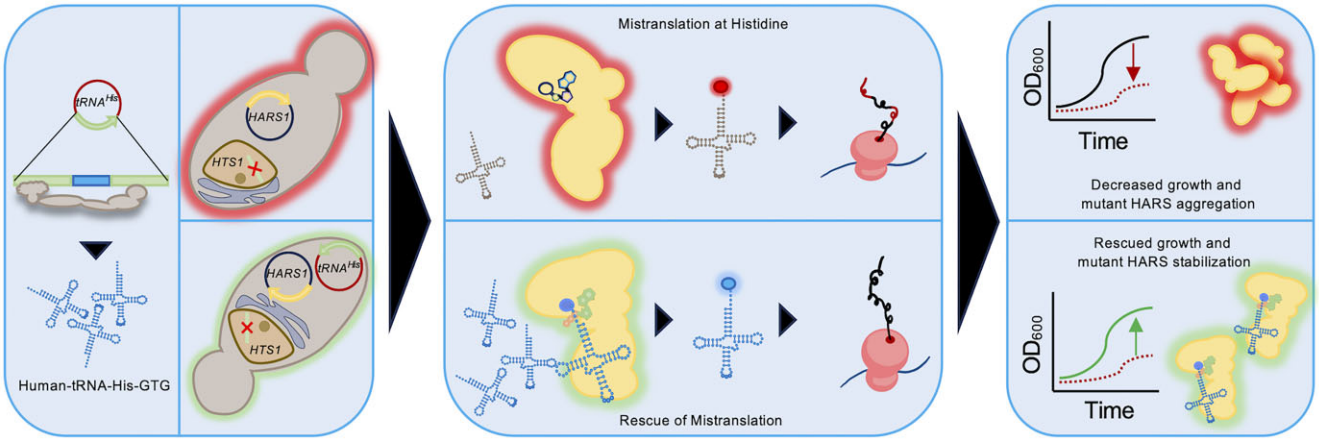

Introduction

Charcot-Marie-Tooth Disease (CMT) is the most commonly inherited peripheral neuropathy, affecting 1 in 2500 individuals (1). CMT is genetically heterogeneous with chronic neuropathy of the distal motor and sensory nerves. Disease onset typically occurs in the first or second decade of life, and current treatment options are limited to the alleviation of CMT related symptoms (2). Over 150 genes have been associated with CMT, with close to 60 known disease-causing alleles found in six different aminoacyl-tRNA synthetases (aaRSs), including glycyl- (GARS) (3), tyrosyl- (YARS) (4), alanyl- (AARS) (5), histidyl- (HARS) (6), methionyl- (MARS) (7) and tryptophanyl- (WARS) (8) transfer RNA (tRNA) synthetases. Mutations in HARS are causative for Charcot-Marie-Tooth disease type 2W (CMT2W), an axonal form of the disease exhibiting autosomal dominant inheritance (9). Most patients

Received: March 15, 2024. **Revised:** September 13, 2024. **Editorial Decision:** October 10, 2024. **Accepted:** October 16, 2024

present clinically with abnormal gait patterns, bony foot deformities and loss of distal sensory function (6). Both loss-of-function and gain-of-function mutations can lead to CMT phenotypes, and the mechanisms may not be mutually exclusive within a disease subtype (9).

The aaRSs family proteins are indispensable in all domains of life and play an essential role in protein synthesis by charging amino acids to their cognate tRNAs (Figure 1A). The fidelity of the genetic code relies on the accurate decoding of messenger RNA (mRNA) codons into amino acids, which relies on precise pairing of each aminoacyl-tRNA anticodon to mRNA codons at the ribosome. One of the most critical steps to ensure translation fidelity is the accurate ligation of amino acids to their cognate tRNAs, since the ribosome does not discriminate against mischarged tRNAs (10). The aaRSs distinguish their cognate tRNA from a large pool of tRNA molecules using identity elements found in the tRNA body (Figure 1A). Similarly, the amino acid binding site in an aaRS generally accommodates only the cognate amino acid, and mutations in the amino acid binding domain can lead to mis-aminoacylation of tRNAs (Figure 1B).

Human HARS is a homodimeric enzyme composed of a catalytic domain, a tRNA binding domain, and a helix-turn-helix domain referred to as WHEP-TRS, which is important in protein–protein interactions such as dimerization or complex formation (Figure 1C) (11). For most aaRSs, the anticodon is a major identity element; however, the HARS identity element in $tRNA^{His}$ is outside of the canonical tRNA body in a diversity of species, including humans and yeast. $tRNA^{His}$ possesses a unique guanylate residue at position -1, which is post-transcriptionally added by $tRNA^{His}$ guanylyl transferase (Thg1) in eukaryotes (12,13). Interestingly, Thg1 recognizes the anti-codon of $tRNA^{His}$ as its primary recognition site, while the G_{-1} residue is required for aminoacylation by HARS. The primary function of HARS is the aminoacylation of $tRNA^{His}$ with the cognate amino acid histidine (His), but moonlighting functions have been identified for HARS, such as a role in leukocyte chemotaxis (14). Circulating HARS is also causative for anti-histidyl tRNA synthetase autoantibodies (anti-Jo1) in one of the most common anti-synthetase syndromes (15).

Human diseases caused by mutations in the HARS protein can result from either loss- or gain-of-function mutations (9). HARS loss-of-function mutations, such as the autosomal recessive Tyr454Ser variant prevalent in an Ontario Amish population, leads to HARS protein instability and reduced histidine incorporation in patient-derived fibroblasts (16,17). Gain-of-function mutations in aaRSs are thought to be caused by defects in aminoacylation that allow for ligation of an incorrect amino acid to the tRNA molecule (Figure 1A,B) producing mistranslated proteins (18). Mistranslation can result in protein misfolding, aggregation and a defective proteome (19,20). Autosomal dominant CMT causing mutations V155G and S356N in the HARS catalytic domain lead to a toxic gain-of-function where a relaxed amino acid specificity causes mistranslation of noncognate amino acids at histidine (His) codons, proteome-wide translation errors, and protein aggregation. In the case of HARS V155G and S356N, supplementation with histidine alleviated growth and mistranslation phenotypes in a humanized yeast model (21). Similarly, CMT causing mutations in GARS and YARS slows translation and reduce global protein production rates; however, these mutations did not lead to a decrease in aminoacylation activity as the disease-causing mechanism (22,23).

We developed a humanized *Saccharomyces cerevisiae* model system to study CMT-causing HARS alleles V133F and Y330C, associated with CMT2W (Figure 1C). Using a model where human HARS complements deletion of *S. cerevisiae* yeast ortholog *HTS1*, we previously showed that HARS alleles V133F and Y330C lead to a significant growth deficiency that cannot be compensated by histidine addition (21). We now show that these CMT mutations lead to HARS protein destabilization and mis-incorporation of amino acids at histidine codons. Mistranslation was rescued by the overexpression of human $tRNA^{His}$, restoring yeast growth to wildtype levels. Our model for $tRNA^{His}$ supplementation in an *S. cerevisiae* yeast model of human HARS variants allows for rapid assessment of $tRNA^{His}$ supplementation to rescue allele-specific disease variants. With rapid advances in tRNA therapeutic applications (24), we anticipate that wildtype $tRNA^{His}$ supplementation will be a promising therapeutic for individuals with CMT2W peripheral neuropathy.

Material and methods

Yeast strain and growth conditions

Generation of yeast models of HARS V133F and and Y330C were described previously (21). Cells were grown on selective synthetic defined (SD) (6.7 g/L yeast nitrogen base, 2% glucose, 60 mg/L L-isoleucine, 20 mg/L L-arginine, 40 mg/L L-lysine, 60 mg/L L-phenylalanine, 10 mg/L L-threonine, 10 mg/L L-methionine and 10 mg/L adenine hemisulfate salt) or yeast-extract-peptone-dextrose (YPD) liquid media (10 g/L yeast extract, 20 g/L peptone and 20 g/L dextrose or 50 g/L of YPD broth), supplemented with 20 g/L agar for solid medium growth. SD medium was supplemented with amino acids as needed for selectivity markers at 60 mg/L L-leucine or 20 mg/L uracil. For growth curves, yeast cultures were grown in SD Leu-medium in 96-well plates for 48 h, and SD Ura- Leu- medium in 96-well plates for 24 h when supplemented with $tRNA^{His}$. For spotting assays, yeast were spotted on SD Leu- or SD Ura^{-} Leu^{-} plates for non-supplemented and $tRNA^{His}$ supplemented cultures, respectively, with 1:1, 1:4, $1:4^2$,$1:4^3$ and $1:4^4$ dilutions. All cultures were grown at 30°C.

Plasmids

Wildtype HARS variants were expressed as a YFP fusion protein from p425-ccdB-GPD (LEU2 plasmid) as described previously (21). To express wildtype HARS and the V133F and Y330C variants, gateway cloning was used to move the previously established variants in the pDONR201 vector to pcDNA3.2 with a C-terminal V5 tag. For co-expression of human $tRNA^{His}$ with HARS in mammalian cells, the tRNA-His-GTG-1–7 gene with 300 bp of the upstream and downstream genomic sequence was amplified using primers binding to genomic DNA extracted from HEK 293T cells. Primers (5′ – GTTCAACATGTCCCCCAAGGGTAGTCTGAGTTC – 3′; 5′ – GTTCAACATGTGTACATGAAAA GAGAAAAAAAT-CACAGGGTCATAG – 3′) included sequences to append *Pci*I cut sites and cloned into the *Pci*I site of pcDNA3.2 through restriction cloning. Human tRNA-His-GTG-1–7 was cloned into p426-GPD (ATCC: 87361) between the 300 bp upstream

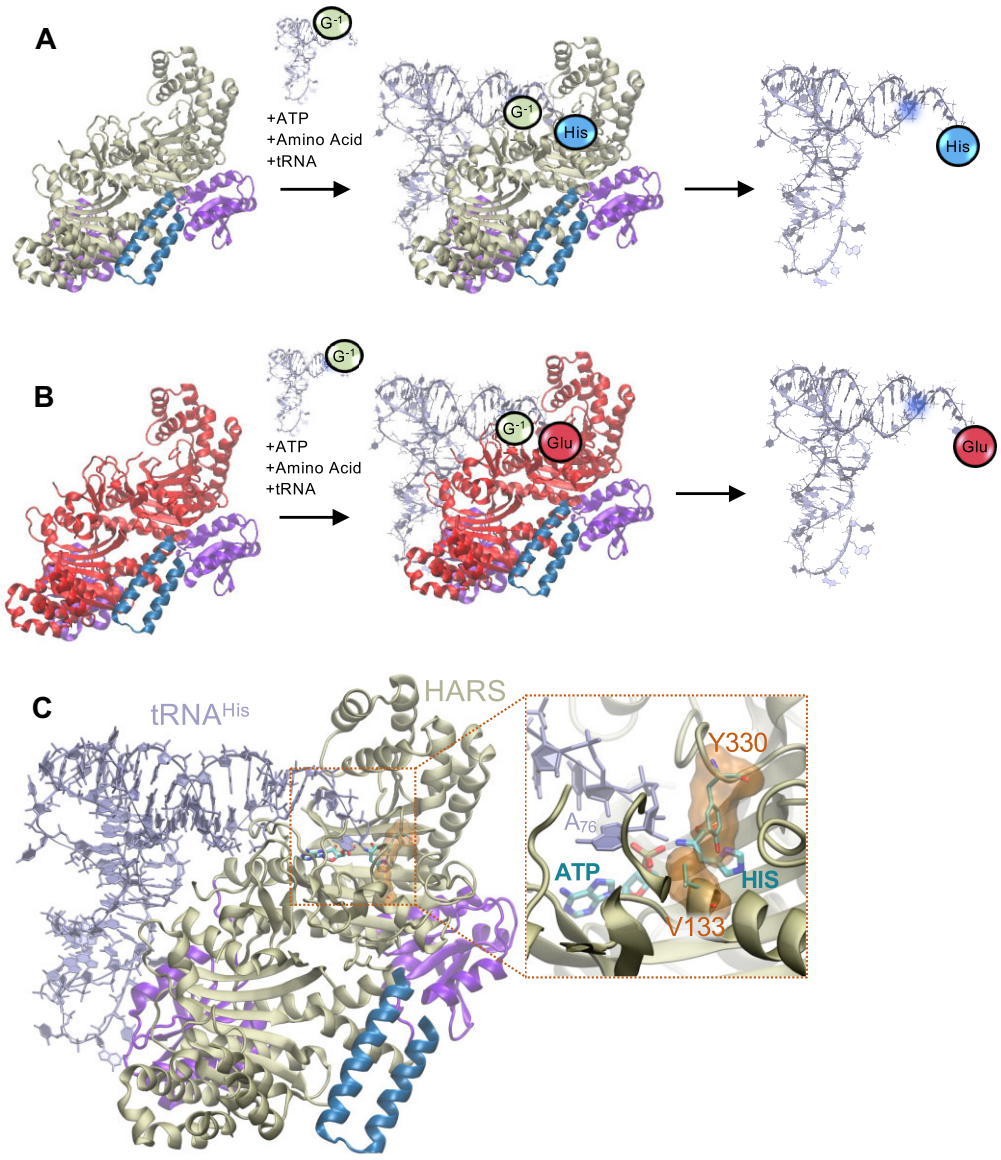

Figure 1. Aminoacylation of tRNA by aaRSs. (**A**) Aminoacylation and (**B**) mis-aminoacylation caused by mutations in the catalytic domain. The HARS G^{-1} identity element on the tRNA is highlighted in green. (**B**) Mutations in the catalytic domain of an aaRS (red) can lead to mis-aminoacylation of tRNA, resulting in mistranslation at the ribosome. (**C**) CMT2W causative alleles Y330C and V133F in HARS structure: Human HARS homodimer (PDB ID: 6O76) with the WHEP domain in blue, catalytic domain in tan and tRNA binding domain in purple. Human HARS was superimposed with the crystal structure from *Thermus thermophilus* in complex with $tRNA^{His}$ (PDB ID: 4RDX), and the tRNA is shown in dark blue, with the 3′ acceptor stem coloured blue. CMT2W HARS mutants V133F and Y330C depicted in orange. Figure generated with PyMOL (Schrodinger, LLC).

and downstream flanking regions for yeast $tRNA^{His}$ to ensure tRNA expression and processing in yeast. The $tRNA^{His}$ construct was synthesized by AZENTA life sciences.

Mammalian cell lines and growth conditions

HEK 293T cells were cultured in DMEM supplemented with 10% FBS in a humidified incubator at 37°C with 5% CO_2. For the CCK8 assay (Abcam, Cambridge, UK), cells were seeded at a density of 5000 cells per well in 96-well plates; for the Cytotox-Glo assay, cells were seeded at a density of 10 000 cells per well. Cells were incubated overnight to allow for proper attachment after seeding.

On the day of transfection, 100 ng of plasmid DNA was diluted in 5 μL of Opti-MEM reduced serum medium (#31985070, Gibco, Thermo Fisher Scientific, Waltham, MA, USA), and 0.24 μL of P3000 reagent (#L3000001, Thermo Fisher Scientific) was added to this mixture. A separate solution was prepared by adding 0.4 μL of lipofectamine 3000 (#L3000001, Thermo Fisher Scientific) to 5 μL of Opti-MEM medium. Both the DNA mixture and the lipofectamine solution were incubated separately at room temperature for 5 min before being combined. After gentle mixing, the combined transfection mix was further incubated at room temperature for 30 min, and subsequently, 10 μL of the transfection mix was added to each well. The plates were shaken for 10 s on an orbital shake setting using a Cytation instrument (BioTek Instruments, Winooski, VT, USA) to ensure even distribution of the transfection mix. The transfected cells were analysed using the CCK8 (Abcam, Cambridge, UK) and Cytotox-Glo assays (Promega Corporation, Madison, WI, USA) according to the manufacturer's instructions.

In vitro transcription and purification of $tRNA^{His}$

A template for *in vitro* transcription of $tRNA^{His}$ was produced through PCR amplification of $tRNA^{His}$-GTG-1–7 from the p426 plasmid to add the T7 promoter (lower case letters) on the 5′ end of the gene (5′-tctagataatacgactcactataGGCCGTGATCGTATAG-3′; 5′-TGGTGCCGTGACTCGGATTCGAACC-3′). The DNA template was purified using the GeneJET PCR purification kit from Thermofisher Scientific according to manufacturer instructions. Run off *in vitro* transcription was performed in 40 mM Hepes/KOH (pH 8.0), 22 mM $MgCl_2$, 5 mM dithiothreitol, 1 mM spermidine and 4 mM of each adenosine triphosphate (ATP), guanosine triphosphate (GTP), cytidine triphosphate (CTP), uridine triphosphate (UTP) and guanosine monophosphate (GMP) with 8 μg/mL of template DNA and 30 nM T7 RNA polymerase. The reaction mixture was incubated at 37°C for 3 h.The product was separated on an 8 M urea, 12% polyacrylamide gel. tRNA was visualized by UV- shadowing and extracted from the gel to to purify the full-length $tRNA^{His}$ product as before (13). Following centrifugation to remove insoluble precipitates, an equal volume of 25:24:1 phenol-chloroform-isoamylalcohol (pH 7.8) was added to the supernatant. The aqueous phase was separated by centrifugation and transferred to an equal volume of ice-cold ethanol with 270 mM NaAcetate pH 5.3. RNA was precipitated at -80°C followed by centrifugation for 30 min at 12 000 x *g* at 4°C. The pellet was washed with cold 95% ethanol and resuspended in RNase free water. To fold the tRNA, the sample was heated to 95°C and slowly cooled in a heat block to room temperature prior to use.

Recombinant HARS purification and protein stability assays.

HARS recombinant protein was produced as a His-tagged fusion protein in *Escherichia coli* and purified by Ni-NTA affinity chromatography as described previously (21). Thermal stability assays were done for V133F as described using full length $tRNA^{His}$ (21,25). Partial tryptic digestion was adapted from an assay established for Glutamyl-prolyl-tRNA synthetase (26) with the following modifications: 2 mg/mL of wildtype or mutant HARS proteins with or without 2 μM $tRNA^{His}$ minihelix were incubated with 2 μg/mL of sequencing grade modified Trypsin (Promega) prepared following manufacturer recommendations. The $tRNA^{His}$ minihelix ((5′-pGGCCAUCCUGCGGGGUGGCACCA-3′) was used as a proxy for full length $tRNA^{His}$. Reactions were incubated at 37°C for 5, 30, 60 or 120 min and quenched with 3X SDS-Dye (6% sodium-dodecyl sulfate (SDS), 30% glycerol, 0.006% bromophenol blue, 125 mM Tris-HCl (pH 6.8)) and boiling at 95°C. Controls (C0 and C120) were incubated without trypsin for 0 or 120 min, respectively. HARS proteins were equilibrated with tRNA, or equivalent volume of buffer, prior to digestion.

Circular dichroism analysis

Samples of HARS proteins were analysed by CD spectroscopy, as described previously (21). Briefly, protein samples were dialyzed into the UV transparent CD buffer (20 mM Tris-H_2SO_4 pH 8.0, 150 mM NaF) and CD spectra were obtained at 2 μM concentrations in a 0.1 cm cuvette. CD spectra were recorded using a Jasco PTC-4235 CD spectrometer at 21°C. The spectra were collected over the 260–190 nm range with a bandwidth of 1 nm. A total of five spectra were recorded for each sample and buffer spectrum was subtracted for baseline correction. Deconvolution of these data to estimate secondary structure composition was determined with ridge regression analysis utilizing CONTINLL with reference set 7 through Dichroweb (27,28).

Northern blotting

Northern blotting was adapted from Varshney *et al.* (29). Briefly, whole cell RNA was extracted from yeast samples using pH 4.5 phenol-chloroform extraction and ethanol precipitation. Whole RNA was separated on an 8 M urea polyacrylamide gel in 0.1 M sodium acetate buffer, pH 5.0, then transferred and fixed to nylon membrane (Amersham Biosciences, RPN303S). Membranes were probed for yeast $tRNA^{His}$ (5′ - CTAGAATCGAACCAGGGTTTCATC – 3′), human $tRNA^{His}$ (5′ –TCGGATTCGAACCGAGGTTGCTGC – 3′) and 5S RNA (5′ – GGTAGATATGGCCGCAACC – 3′) with digoxigenin (DIG) labelled probes prepared according to manufacturer instructions (Roche Applied Science, Cat. No. 11745832910). DIG labels were detected using anti-digoxigenin-AP-conjugate antibody and NBT/BCIP (Roche Applied Science, Cat. No. 11093657910) and imaged using the ChemiDoc MP Imaging system from Bio-Rad.

Yeast sedimentation assay and western blotting

Sedimentation assays were adapted from Shiber *et al.* (30). Briefly, yeast cultures were normalized to $A_{600} = 1.0$ and lysed in an 8 M urea, 1% SDS, 10 mM MOPS, 10 mM EDTA buffer and fractionated into whole lysate, supernatant (soluble proteins) and pellet (insoluble proteins). To determine HARS abundance in each fraction, samples were separated by 12% SDS- Polyacrylamide gel electrophoresis (PAGE) and transferred to polyvinylidene fluoride (PVDF) membrane (Roche Applied Science, Cat. No. 03 010 040 001). Anti-GFP antibody (ab32146) was used at a ratio of 1:1000. Secondary antibody IRDye® 800CW Goat-anti-Rabbit IgG (LiCor, 926 – 32 211) was used at a ratio of 1:10 000 and detected using the ChemiDoc MP Imaging system from Bio-Rad.

Mass spectrometry

Sample preparation for MS analysis

Yeast cells were lysed in 100 mM Tris-HCl (pH 7.5), 200 mM NaCl with manual glass bead disruption. In-solution digest samples were prepared for Liquid Chromatography with tandem mass spectrometry (LC-MS/MS) analysis at Bioinformatics Solutions Inc. (Waterloo, Ontario, Canada). Briefly, samples were reduced with 10 mM dithiothreitol (Sigma-Aldrich, Missouri, USA), alkylated with 20 mM iodoacetamide (Sigma-Aldrich, Missouri, USA) and precipitated in acetone at −80 °C. After removing the acetone, the samples were then digested overnight with MS grade trypsin (Promega, Wisconsin, USA). Digested peptides were desalted with in-house made C18 spin columns. The desalted samples were dried down and kept in −20°C until analysis.

Samples were resuspended in 0.1% formic acid prior to MS analysis. For each run, the resuspended sample was separated by nanoflow liquid chromatography using an Ultimate 3000 chromatography system (ThermoFisher, Massachusetts, USA), then injected into the Thermo Orbitrap Exploris 240 (ThermoFisher, Massachusetts, USA). Liquid chromatography was

performed using a constant flow of 0.25 μL/min and a 15 cm reversed-phased column with a 75 μm inner diameter filled with Reprosil C18 (PepSep, Bruker, Germany). Mobile phase A was 0.1% formic acid and Mobile phase B was 99.9% acetonitrile, 0.1% formic acid. The separation was carried out over 120 min as follows: linearly 4% B to 32% B over 110 minutes with an increase to 95% B over 0.1 min and held constant for 4.9 min to clean the column. Then the B percentage was set back to 4% in the final 5 min.

Bottom-up MS data analysis

MS/MS data acquired on Thermo Orbitrap Exploris 240 for each sample were carried out in data-dependent acquisition mode with a cycle time of 3 s. In the first round, MS1 scan data were obtained at 60 000 resolution (at 400 m/z) with a mass range of 400–1600 m/z. The automatic gain control (AGC) was set to standard, with an auto maximum ion injection time. The radio frequency (RF) lens was set to 70%. The charge state filter was set to 2–8, and the dynamic exclusion was set to 20 s. Isolation for MS2 scans was performed in the quadrupole, with an isolation window of 0.7 Da. MS2 scan data were acquired at a resolution of 15 000 m/z in the orbitrap, with a standard AGC target and an auto ion injection time. The scan range of MS2 was also set to auto. Higher energy collisional dissociation (fixed normalized collision energy: 30%) was used for generating MS2 spectra, with the number of microscans set to 1.

Proteomics data search

MS Raw Files were processed using PEAKS Studio 11.5 (Bioinformatics Solutions Inc., Ontario, Canada). The data were searched against the reviewed *Saccharomyces cerevisiae* Uniprot database. Precursor ion mass error tolerance was set to 10 ppm and fragment ion mass error tolerance was set to 0.02 Da. Semi-specific cleavage with trypsin was selected with a maximum of two missed cleavages. A fixed modification of carbamidomethylation (+57.02 Da) on cysteine residues and variable modifications of deamidation (+0.98 Da) on asparagine and glutamine, as well as oxidation (+15.99 Da) on methionine were specified. A 1% false discovery rate (FDR) was set for the database search. After the database search, additional variable modifications were searched to identify mutations. The mutations and corresponding mass shifts are as follows: E to H (+8.02), H to E (-8.02), H to Q (-9.00), Q to H (+9.00), H to Y (+26.00), Y to H (-26.00), H to T (-36.01) and T to H (+36.01). Only mutations supported by relative fragment ion intensities >2% and having a PEAKS AScore of >15 were considered in the analysis.

Statistical analysis

All statistical significance was determined using t-tests to compare the means and standard deviations of the control data and the experimental data sets, or a one-way ANOVA test for multiple comparisons as indicated. Statistical significance levels are annotated using asterisks (**** $P < 0.0001$, *** $P < 0.001$, ** $P < 0.01$, * $P < 0.05$, ns = not significant).

Results

Mutations in aaRSs can manifest in a variety of diseases, which can be attributed to reduced aaRS stability, activity, altered amino acid or tRNA recognition or non-canonical functions (18). Here, we analyse the impact of two CMT-causing HARS mutations, V133F and Y330C (Figure 1C). We previously generated a humanized yeast model of these mutants, where endogenous yeast HARS is deleted and either human wildtype or a pathogenic allele is expressed from a plasmid. We found that V133F and Y330C lead to a strongly reduced growth phenotype in yeast, and in contrast to that, HARS mutants S356N and V155G, histidine supplementation did not rescue the growth defect. Indeed, histidine supplementation appeared to have a detrimental effect on the yeast model, with increased protein aggregation upon histidine supplementation (21).

HARS V133F and Y330C lead to protein misfolding and a growth phenotype in yeast.

While HARS V133F and Y330C mutations clearly cause a growth phenotype in yeast, the underlying mechanism remained unclear (21). Yeast dependent on mutant HARS V133F or Y330C showed reduced growth rates and significantly increased doubling times by 1.2-fold for V133F and 1.4-fold for Y330C (Supplementary Figure S1A,B) compared to yeast cells dependent on wildtype HARS.

To test if this phenotype is caused by reduced protein stability or structural changes, we purified recombinant HARS proteins from *E. coli* and probed for structural differences that may underlie the disease pathology. Limited tryptic digestion was previously used as a measure of subtle changes in protein structure in glutamyl-tRNA synthetase (26), and we employed this method to probe for differences in wildtype HARS, HARS V133F and HARS Y330C proteins. The limited tryptic digest revealed a differential digest pattern for V133F, but not Y330C relative to wildtype HARS (Figure 2A). For wildtype HARS, the major 55 kDa fragment (arrow 1) is apparent within 30 min, and cleavage progressed to yield one major cleavage product at 120 min and several minor peptides (arrow 2). In V133F HARS, cleavage peptide products appear within the first 5 min and the cleavage pattern is distinct from wildtype HARS, with fragments missing (arrow 2) and another separate one appearing (arrow 3). V133F does not produce the same major cleavage product at 120 min that is apparent on the wildtype protein (arrow 1). The cleavage pattern of Y330C more closely resembles the wildtype protein, leading to the same major cleavage product formation, but faster cleavage is observed after 5 min (arrow 4), and an additional band is present after 120 min (arrow 5). These changes in cleavage pattern are consistent with subtle (Y330C) and more significant (V133F) changes in tertiary structure (31). The tryptic digest suggests subtle changes in structure that may be due to increased flexibility between motifs, allowing different cut sites to be more rapidly accessed by trypsin and thus more rapid degradation of the protein.

Interestingly, we found that soluble endogenous $tRNA^{His}$ abundance is increased in Y330C compared to wildtype HARS yeast (Figure 2C and D), indicating a role for tRNA abundance or tRNA binding in the phenotype. Changes in tRNA abundance may be indicative of tertiary structure changes in aaRS proteins leading to altered tRNA binding (31). We used differential scanning fluorimetry (25) to analyse whether the changes in Y330C structure impact protein stability (Figure 2B, Supplementary Figure S3). We had previously characterized wildtype HARS and V133F (21), and have included these data for comparison in Figure 2B. Interestingly,

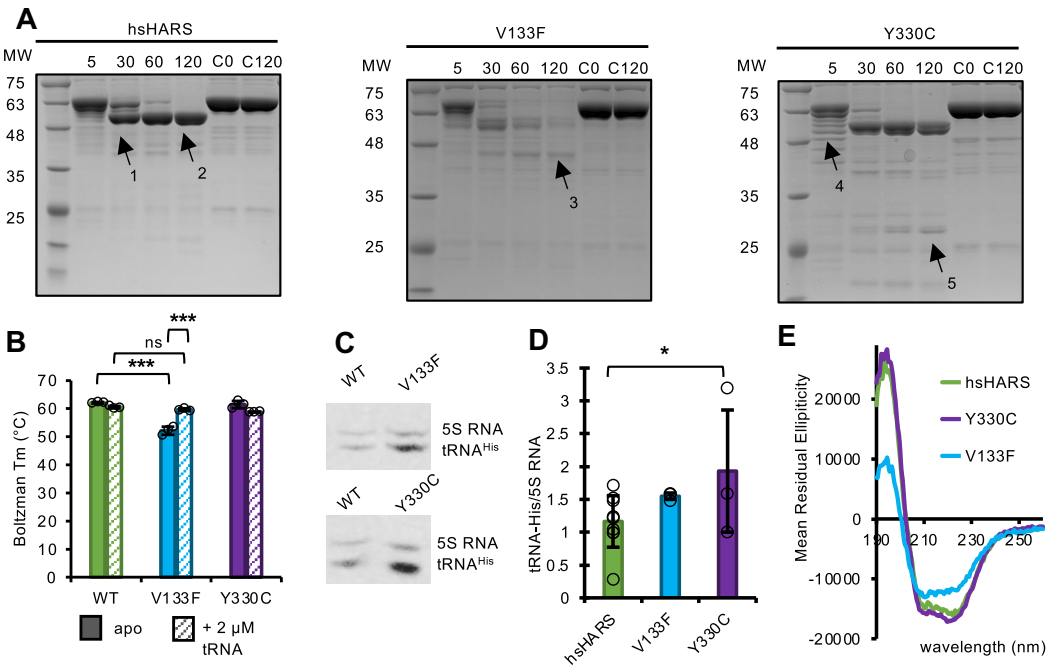

Figure 2. HARS V133F and Y330C induce a growth phenotype in a humanized yeast model of HARS disease. A) Limited tryptic digestion of HARS proteins. HARS wildtype and mutant proteins were equilibrated with buffer then subjected to digestion by trypsin at 37°C for the time indicated in minutes. Control samples of HARS were incubated without trypsin for 0 or 120 min (C0 and C120). The reactions were quenched with SDS dye and boiling, then separated on a 12% denaturing SDS-polyacrylamide gel followed by staining with Coomassie blue to visualize digest products. The expected mass of 6x-His tagged HARS is approximately 58 kDa. Soluble whole cell RNA from hsHARS, V133F and Y330C mutant yeast was extracted and purified under acidic conditions and separated on an 8M urea gel. (**B**) Protein thermal stability of recombinant HARS WT or mutants with or without 2 µM $tRNA^{His}$ minihelix. Purified protein was incubated with tRNA and heated from 25°C to 95°C, measuring fluorescence intensity to follow protein unfolding. The melting temperature (Tm) was determined by fitting fluorescence intensity of three biological replicates per condition to the Boltzmann equation in the Protein Thermal Shift software. Soluble whole cell RNA from hsHARS, V133F, and Y330C mutant yeast was extracted and purified under acidic conditions and separated on an 8 M urea gel. (**C**) Northern blot and (**D**) ratio of soluble $tRNA^{His}$ to 5S RNA of blots for yeast $tRNA^{His}$. Blots were imaged using the ChemiDoc MP imaging system and quantified using ImageLab. (**E**) CD spectra of purified recombinant WT, V133F and Y330C proteins.

despite differences in the secondary and tertiary structure detected by CD spectroscopy and the limited tryptic digest, the Y330C mutation does not impact recombinant protein stability (Supplementary Figure S2). Since Y330C leads to increased tRNA abundance in yeast, we tested whether the addition of full length tRNA had an impact on the melting temperature of Y330C, but this was not the case, the melting temperature for Y330C was indistinguishable from wildtype HARS under all conditions. Excitingly, V133F caused a decrease in melting temperature by about 10°C (21), but the addition of full length tRNA restored thermal stability to wildtype levels (Figure 2B). To test if tRNA addition would impact the limited tryptic digest, we incubated the recombinant HARS proteins with a $tRNA^{His}$ minihelix (21), prior to digestion. The minihelix was used as a proxy for full length $tRNA^{His}$ and was previously shown to be a competent substrate for HARS (32) and effective in thermal stability assays (21). We observed no changes in the tryptic digest pattern (Supplementary Figure S1C–E).

CD spectroscopy of the HARS proteins further highlighted the structural differences of V133F and the closer resemblance of Y330C to wildtype protein (Figure 2E). Ridge regression analysis suggested the wildtype HARS protein has 49% alpha helical content with a low abundance of beta strands and turns, and the remaining regions being unfolded or disordered (Figure 2E, Table 1). V133F had a substantial reduction in alpha helices, estimated at 19% lower than the wildtype HARS protein. Correspondingly, the beta strand and unfolded content were estimated to increase by 10% and 8%, respectively in V133F. Taken together, the changes in proteolytic digestion patterns and estimated secondary structure content indicate that the V133F HARS mutation alters protein folding, providing a potential source for the aberrant enzymatic function observed in the disease phenotype. Overall, our biochemical analysis revealed significant structural differences for both Y330C and V133F relative to the wildtype HARS protein.

HARS mutations V133F and Y330C lead to a perturbance of the proteome.

Both V133F and Y330C mutations show a significant decrease in growth phenotype, and we previously showed that both variants lead to the accumulation of insoluble proteins, especially when grown under increased histidine concentrations in the media (21). To evaluate the impact of these mutations on the yeast proteome, we performed label-free mass spectrometry on cells grown under normal histidine concentrations (Supplemental Data File 1). When compared to wildtype human HARS expressing cells, we found a significant change in abundance by at least 2-fold for 16 proteins in cells expressing V133F, and 118 proteins differentially abundant in cells with HARS Y330C (Figure 3A–D). Data and analysis for each protein that was significantly changed by more than 2-fold in abundance is in Supplemental Data File 2. Of these, V133F showed eight proteins increased in abundance and eight decreased relative to cells with wildtype HARS, while

Table 1. HARS secondary structure as predicted by CD spectroscopy data analysis

HARS Mutation	Helix1	Helix2	Strand1	Strand2	Turns	Unordered	Total
WT	29%	20%	2%	5%	16%	28%	100%
Y330C	29%	18%	7%	6%	17%	23%	100%
V133F	17%	13%	10%	7%	17%	36%	100%

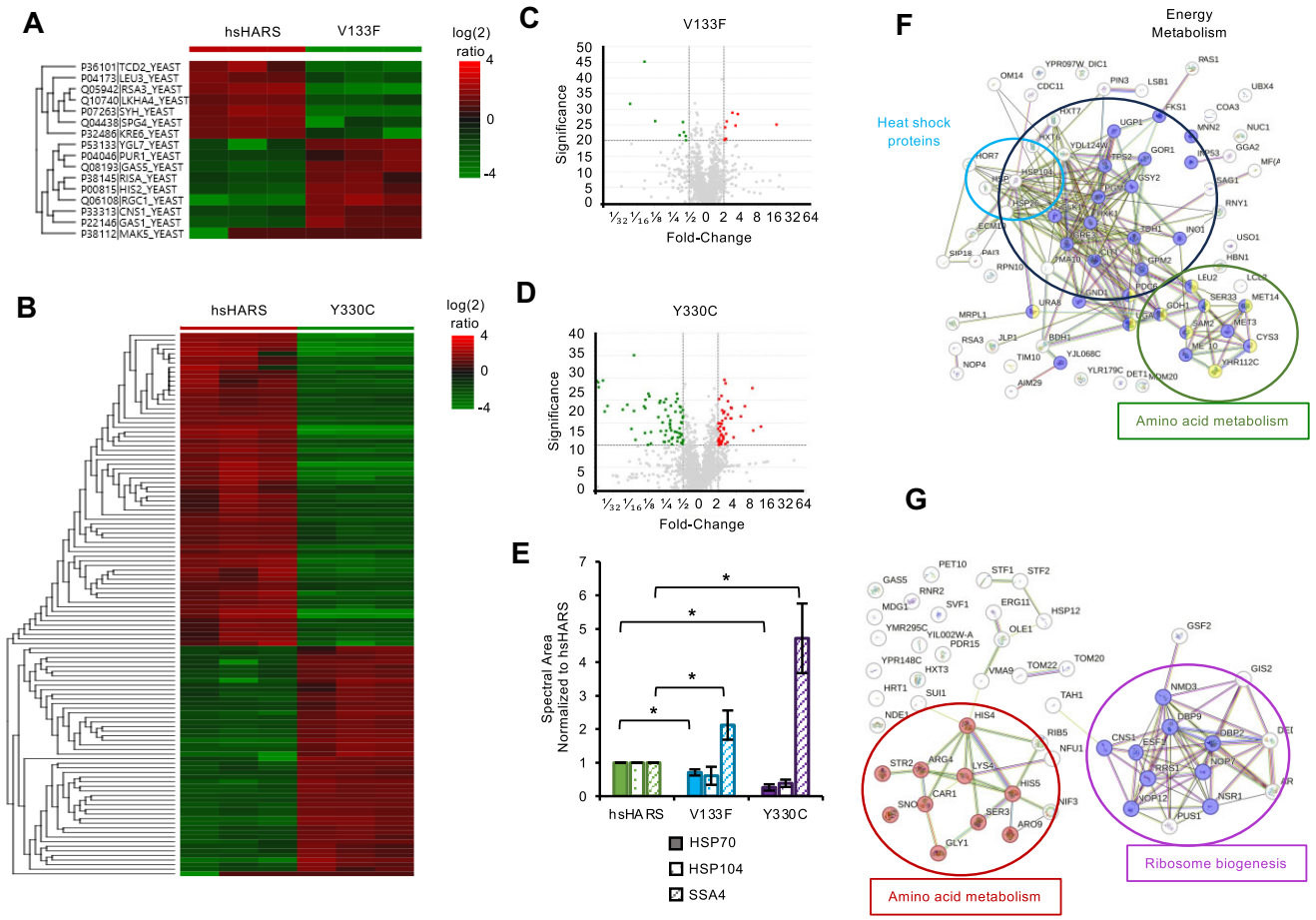

Figure 3. V133F and Y330C change the composition of the proteome in yeast. Heat maps of differentially abundant proteins identified by label-free quantification proteomic analysis between yeast expressing wildtype HARS or (**A**) V133F or (**B**) Y330C HARS. Volcano plots of proteins with significant changes shown for (**C**) V133F and (**D**) Y330C HARS, with upregulated proteins identified in red and downregulated proteins identified in green. String diagram of proteins (**E**) downregulated and (**F**) upregulated in Y330C compared to wildtype. (**G**) Bar graph of heat shock proteins changed in abundance in Y330C and V133F normalized to wildtype HARS expressing yeast.

Y330C showed an increase in abundance for 49 proteins, and 69 proteins were decreased in abundance.

To identify pathways most impacted by these mutations, we performed a protein–protein interaction analysis using the search tool for retrieval of interacting genes (STRING) (33). For V133F, no functional enrichment of the 16 differentially abundant proteins was identified (Supplementary Figure S3), which is not surprising given the limited number of differentially abundant proteins. It is interesting to note, however, that the heat shock protein 70 (HSP70), one of the proteins involved in the response to proteomic stress, is activated by 2.1-fold in the V133F cells, whereas other heat shock proteins like HSP104 and SSA4 remain unchanged (Figure 3E). This indicates that while V133F shows a clear growth defect, only minor, but significant changes occur in the proteome.

For Y330C, we found a significant downregulation of energy metabolism (KEGG identified Metabolic pathways Gene count 28, FDR 1.34e-07), as well as cellular amino acid metabolic processes (GO:0006520, 11 genes counted, FDR 0.0175) (Figure 3F). Proteins from amino acid metabolism pathways, including cysteine biosynthesis CYS3 (2.3-fold reduction in Y330C) and SAM2 (2.2-fold reduction in Y330C), serine biosynthesis (3-phosphoglycerate dehydrogenase and alpha-ketoglutarate reductase, SER33, 2-fold reduction in Y330C), leucine biosynthesis (beta-isopropylmalate dehydrogenase, LEU2, 4.3-fold reduction in Y330C) and methionine metabolism (Adenylylsulfate kinase, MET14, disaggregase; and ATP sulfurylase MET3, 5-fold reduction in Y330C). In addition, several heat shock proteins were decreased in abundance, including HSP104 (2.1-fold reduction in Y330C), HSP26 (16.7-fold reduction in Y330C) and HSP30 (20-fold

reduction in Y330C), and SSA4 is also significantly downregulated by 3.6-fold, indicating that the unfolded protein response is not activated in these cells. Interestingly, when we performed a STRING analysis of proteins upregulated in Y330C, we found ribosome neogenesis proteins were significantly enriched as well as proteins in amino acid biosynthesis pathways (GO:0006520, gene count 10, FDR 0. 0.0173) (Figure 3G). Proteins in amino acid metabolism that were significantly upregulated included, including proteins in serine, lysine and arginine biosynthesis pathways (see Supplemental File 2) and two proteins in histidine metabolism. HIS5 catalyses the seventh step in histidine biosynthesis (34) (2.7-fold upregulated in Y330C) and HIS4 catalyses the second, third, ninth and tenth steps in histidine biosynthesis (35) (3-fold upregulated in Y330C). Finally, we found that similar to V133F, HSP70 was upregulated by 4.7-fold in Y330C (Figure 3E). These data indicate that Y330C causes substantial changes to protein levels that impact amino acid metabolism and protein quality control pathways.

HARS mutations V133F and Y330C cause mistranslation in yeast.

Our biochemical and proteomic analysis suggests that both Y330C and V133F impact translation fidelity, with V133F causing structural changes and decreased thermal stability in the HARS protein. While this phenotype could lead to a loss of function and reduced aminoacylation activity in the cell, it could also lead to a toxic gain-of-function, especially considering that both mutations are localized in the active site of the protein (Figure 1C). In addition, we previously showed that histidine supplementation exacerbates the growth defect for Y330C and causes increased protein aggregation for both mutants (21). To test whether Y330C and V133F mutants lead to mistranslation, we used bottom-up mass spectrometry to analyse the proteome of humanized yeast that depend on wildtype, V133F or Y330C HARS for growth.

Not surprisingly and indicative of basal error in protein synthesis, some mistranslation events were detected in cells expressing WT HARS, with 18 uniquely mistranslated peptides identified with relative fragment ion intensities >2% and a PEAKS score > 15 (Figure 4). In V133F cells, we observed 2.5-fold more mistranslated peptides, with 49 unique mistranslated peptides total, 26 resulting from mistranslation of glutamine and 17 from tyrosine incorporation at histidine codons, respectively (Figure 4). Interestingly, we identified four cases of histidine incorporation at glutamic acid codons (Supplementary Figure S4). Similar patterns of translation error were observed in Y330C proteome samples where we observed 52 unique mistranslated peptides, including 33 cases of mistranslation of histidine to glutamine and 17 cases of histidine to tyrosine incorporation (Figure 4E). Again, we also observed two peptides with mis-incorporation of histidine at glutamic acid codons (Supplementary Figure S5). These data show a 2.5-fold increase in mistranslation across the proteome in both Y330C and V133F compared to wildtype HARS expressing yeast.

Human tRNA^{His} expression is not toxic to yeast.

Since our biochemical data show that tRNA^{His} stabilizes the V133F protein and restores protein stability to wildtype levels, we proceeded to test whether tRNA supplementation would rescue the growth phenotype in yeast. Yeast tRNA^{His} and human tRNA^{His} have 18 nucleotide changes between the *S. cerevisiae* tRNA^{His}-GTG-1–1 and human tRNA^{His}-GTG-1–7 (Figure 5A) (36,37). We first tested human tRNA^{His} expression in a wildtype yeast background to assess toxicity. No difference in growth was observed compared to no vector or empty vector controls (Figure 5B,C, Supplementary Figure S6A).

While hsHARS complements the deletion of yeast ortholog *hts1,* the humanized yeast model shows reduced growth compared to yeast with endogenous HARS (21). Yeast HTS1 encodes both mitochondrial and cytosolic HARS. Yeast HTS1 has two translation start sites, which are located 60 bp (20 amino acids) apart, resulting in 2 different HARS proteins (38). The longer HARS is localized to the mitochondria. Surprisingly, while deletion of the upstream ATG codon in the *HTS1* transcript results in a respiratory deficient phenotype in *S. cerevisiae*, it does not alter cytoplasmic levels of HARS or reduce viability (38). This suggests that yeast can compensate for the absence of a mitochondrial HARS without a detectable growth phenotype, and that another mechanism is present to compensate for the missing mitochondrial synthetase. Nonetheless, it is evident that human HARS cannot completely complement for yeast HTS1, which may be due to either differences in tRNA^{His}, or the inability of human HARS to compensate for the absence of mitochondrial HTS1. Interestingly, when the expression plasmid for human tRNA^{His} was introduced into both the wildtype BY4742 and the haploid *Δhts1* strain, addition of human tRNA-His-GTG-1–7 gene resulted in a significant increase in growth in the hsHARS yeast strain at both normal and high histidine concentrations (Figure 5D,E), with a significant increase in mean gray area of 3.6- and 4.5- fold, respectively (Figure 5D,E). No significant increase in fluorescence from the hsHARS-YFP protein was noted under normal or high histidine conditions (Supplementary Figure S5B,C).

To further identify changes in the proteome caused by tRNA supplementation, we performed label-free proteomics on tRNA^{His} supplemented cells and compared the proteome to cells expressing wildtype human HARS (Figure 5F). We found seven proteins were significantly upregulated by at least 2-fold in tRNA supplemented cells, and 16 proteins were significantly downregulated by at least 2-fold. We again analysed up and downregulated proteins by STRING and found no significantly enriched pathways were upregulated (Supplementary Figure S5D). Interestingly, four proteins associated with amino acid metabolism were downregulated (Figure 5G), of which three are subunits of mitochondrial glycine decarboxylase complex, GCV1,2 and 3 (all∼ 2.5-fold downregulated in tRNA^{His} supplemented cells). In addition, ARO9 is an aminotransferase involved in tyrosine, phenylalanine and methionine metabolism (2.3-fold downregulated tRNA^{His} supplemented cells). These data indicate that wildtype tRNA^{His} overexpression is well tolerated and even beneficial to yeast cells.

Over-expression of tRNA^{His} rescues HARS V133F and Y330C growth defects.

With successful expression of tRNA^{His} in the wildtype HARS yeast model, we aimed to restore growth in HARS variants V133F and Y330C with tRNA^{His} supplementation. Indeed, tRNA^{His} led to a rescue of growth for both alleles (Figure 6A–C). Doubling times of both alleles V133F and Y330C were

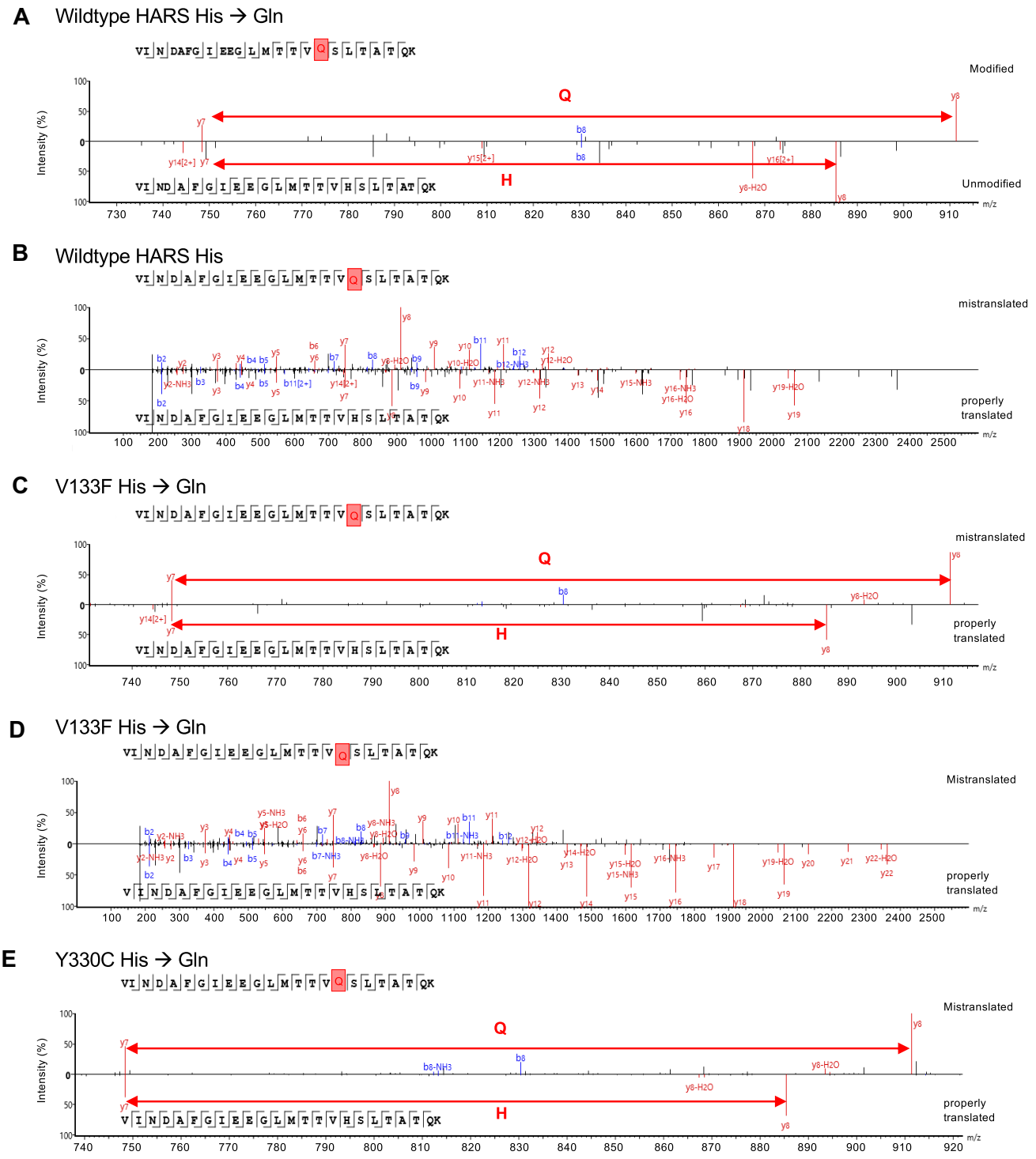

Figure 4. HARS V133F and Y330C lead to mistranslation. Tandem mass spectra are shown for peptides that represent histidine to glutamine mistranslation difference in Y ions highlighted for (**A**) hsHARS, (**C**) HARS V133F and (**E**) HARS Y330C. Mirror plots of the same peptides for (**B**) HARS V133F and (**D**) HARS Y330C showing histidine to glutamine mistranslation.

decreased by 1.7-fold (Figure 6C). Growth was restored by tRNA supplementation under normal histidine and high histidine conditions (Figure 6A,B). Expression of human $tRNA^{His}$ was confirmed by northern blotting, where endogenous yeast tRNA-His-GTG-1–1 was detected in RNA extracts from all yeast strains and human tRNA-His-GTG-1–7 was found only in those carrying the plasmid for its expression (Figure 6D). Following supplementation with tRNA, the doubling time in liquid growth curves and mean gray are of spotting plates of humanized yeast strains expressing V133F and Y330C are indistinguishable from wildtype expressing yeast strains (Figure 6C, E, F), indicating a full restoration of mutant HARS activity. Furthermore, supplementation with high histidine had no significant impact on the growth of the yeast

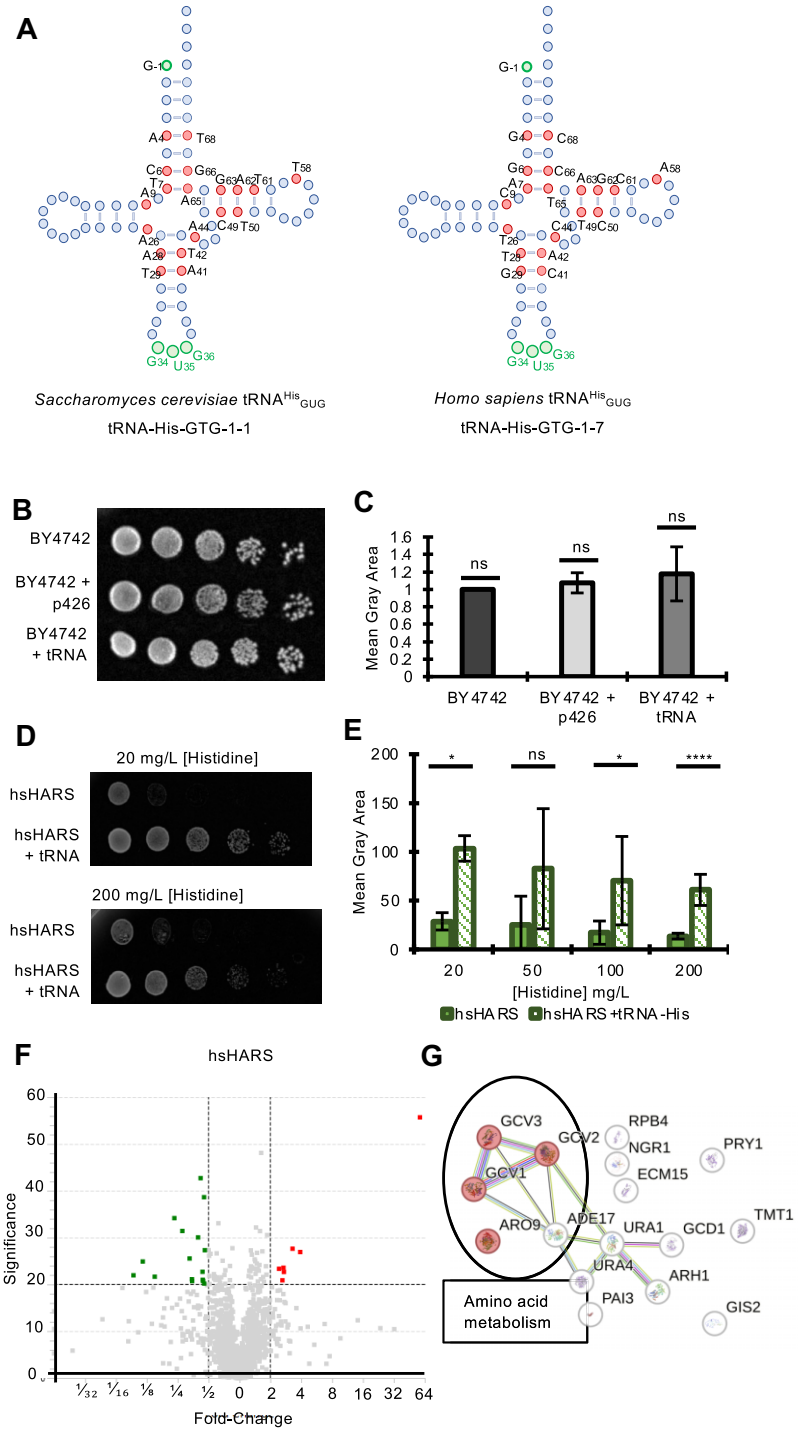

Figure 5. Supplementation with human tRNA^{His} is not toxic and improves growth of yeast strains expressing hsHARS. (**A**) Structure and sequence differences from *Saccharomyces cerevisiae* and human tRNA^{His}. (**B**) Spotting yeast growth assay at 30°C and (**C**) quantification of wildtype yeast overexpressing tRNA^{His}. Yeast strains (BY-4742) with no plasmid, high copy number vector p426, and p426 encoding human tRNA^{His} for yeast expression were grown in YPD medium, normalized to A_{600} = 1.0 and serially diluted 1:1, 1:4, 1:42, 1:43 and 1:44. Three biological replicates were incubated at 30°C for 3 days. (**D**) Spotting assay at 30°C and (**E**) quantification of humanized yeast. ΔHTS1 yeast strains (BY-4742) with a plasmid expressing hsHARS and a plasmid expressing human tRNA^{His} were grown in SD Leu- or SD Ura- Leu-, respectively, normalized to A_{600} = 1.0 and serially diluted as previously described. Three biological replicates each were spotted on complete SD medium with either 20 or 200 mg/L histidine and incubated at 30°C for 4 days. Spotting plates were imaged using the ChemiDoc MP imaging system and quantified using ImageJ. (**F**) Volcano plot of label free proteomic analysis comparing wildtype humanized HARS with tRNA supplemented humanized HARS yeast. (**G**) String maps of differentially expressed proteins in hsHARS yeast cells supplemented with tRNA show downregulated proteins in tRNA supplemented cells compared to unsupplemented cells.

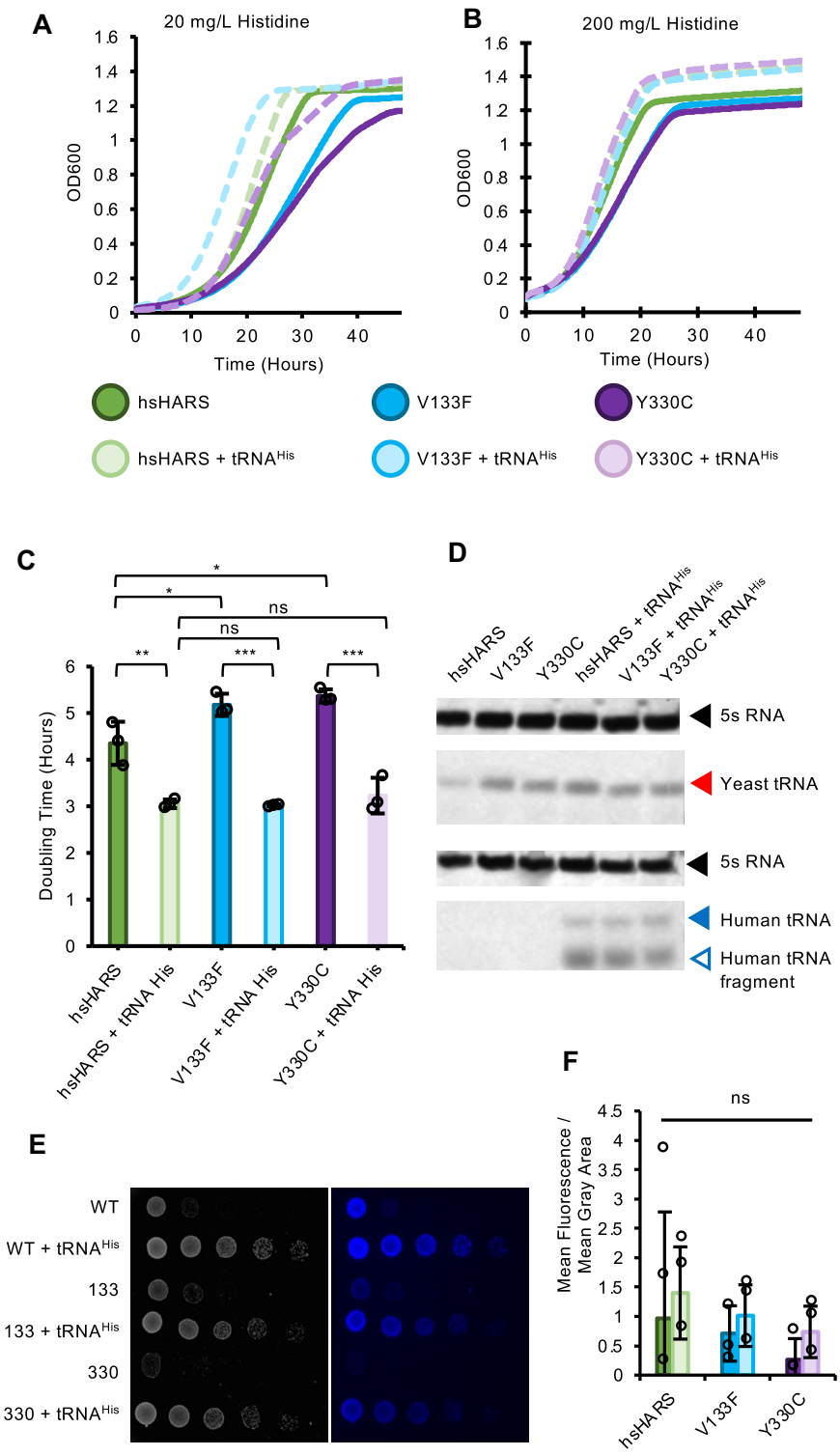

Figure 6. tRNA^{His} supplementation restores growth in HARS V133F and Y330C dependent yeast. Growth curve under (**A**) normal (20 mg/L) and (**B**) high (200 mg/L) histidine conditions and (**C**) doubling time of haploid ΔHTS1 yeast (BY-4742) with high (p425) copy number plasmids expressing wildtype or mutant human HARS. Yeast cultures were grown at 30°C in SD Leu$^-$ for non-supplemented or SD Ura$^-$ Leu$^-$ medium for tRNA^{His}-supplemented cultures in a 96-well plate for 48 h with 10-min read intervals, with three biological and three technical replicates each. The error bars represent one standard deviation of the mean. (**D**) Northern blot for *S. cerevisiae* tRNA^{His} and human tRNA^{His} from yeast cultures used for growth curve experiment under normal (20 mg/L) histidine conditions. Soluble whole cell RNA from hsHARS, V133F and Y330C mutant yeast was extracted and purified under acidic conditions and separated on an acidic 8 M urea gel. A probe for the 5S RNA was used as loading control. (**E**) Spotting yeast growth assay at 30°C and (**F**) quantification. ΔHTS1 yeast strains (BY-4742) with a plasmid expressing hsHARS and a plasmid expressing human tRNA^{His} were grown in SD Leu$^-$ or SD Ura$^-$ Leu$^-$, respectively, normalized to A_{600} = 1.0 and serially diluted as previously described. Three biological replicates each were spotted on complete SD medium with 20 mg/L histidine and incubated at 30°C for 4 days. Spotting plates were imaged using the ChemiDoc MP imaging system and quantified using ImageJ. Error bars represent one standard deviation of the mean.

strains supplemented with tRNA in a dose response experiment (Supplementary Figure S6). These data indicate that Y330C and V133F growth phenotypes can be rescues by cognate human $tRNA^{His}$ expression.

$tRNA^{His}$ supplementation is not toxic to human cells

To test if pathogenic HARS overexpression produced a comparable phenotype in human cells, we expressed wildtype, V133F and Y330C HARS alleles in HEK 293T cells and conducted cytotoxicity and cell viability assays, measured at 6, 24, 48 and 72 h after transfection. Interestingly, while neither HARS allele produced a measurable cytotoxic effect over 72 h (Supplementary Figure S7A), cell viability of V133F expressing cells was greater than wildtype or Y330C expressing cells. This indicates that overexpressing these HARS alleles in HEK 293T cells does not generate a tractable disease model. Nonetheless, we tested if $tRNA^{His}$ expression is toxic to HEK 293T cells in combination with wildtype, V133F and Y330C HARS alleles and high histidine supplementation for Y330C. For almost all conditions, no significant difference in cell viability or cytotoxicity was observed (Supplementary Figure S7C–F), with exception of the growth advantage of the V133F variant over wildtype HARS as nited above. Notably, histidine supplementation had a favourable effect in cytotoxicity at 6 h for all Y330C and wildtype HARS alleles (not tested on V133F), and $tRNA^{His}$ expression was not toxic under any conditions for any alleles (Supplementary Figure S7C–F). Overall, these data show that an overexpression system in human cells does not generate a suitable disease model, but $tRNA^{His}$ overexpression is not toxic.

$tRNA^{His}$ supplementation reverses changes in proteome composition in V133F and Y330C

Since V133F and Y330C caused proteomic changes compared to human wildtype HARS expressing cells, we sought to identify if these changes could be reversed by $tRNA^{His}$ supplementation and performed label-free mass spectrometric analysis of tRNA supplemented cells. Indeed, when comparing the proteomes of $tRNA^{His}$ supplemented hsHARS expressing cells with $tRNA^{His}$ supplemented V133F and Y330C cells, we found a stark reduction in changes to protein levels (Supplementary Figure S8). Additionally, we observe a clear difference in the expression profiles of unsupplemented and supplemented mutants (Supplementary Figure S8A–E) and a stronger correlation of protein abundances of supplemented cells to wildtype (Supplementary Figure S9). A total of nine proteins were changed (down from 16 with no tRNA) in abundance in V133F + $tRNA^{His}$ compared to the wildtype control (Figure 7A, Supplementary Figure S10A), and 42 proteins (down from 116 with no tRNA) were differentially abundant in Y330C + $tRNA^{His}$ compared to the wildtype control with 11 proteins up and 31 proteins downregulated (Figure 7B, Supplementary Figure S10B). When performing functional enrichment studies using STRING, no functional enrichment of these proteins was found for either allele (Supplementary Figure S10C–F). When comparing the number of proteins changed in the mutant strains compared to their tRNA supplemented counterparts (Figure 7C), it is evident that the significantly changed proteome is reduced by at least 50%.

Since one of the most changed networks in Y330C cells was in amino acid metabolism, we plotted the abundance changes of all proteins involved in amino acid metabolism that were significantly changed under any condition and visualized these changes in a heat map normalized to the proteome of unsupplemented wildtype human HARS (Figure 7D). It is evident that proteins upregulated in V133F and Y330C mutants (red) are returned to expression levels comparable to hsHARS $tRNA^{His}$ supplemented cells upon expression of $tRNA^{His}$. Similarly, most proteins that are decreased in abundance in the mutants are restored to wildtype levels once cognate $tRNA^{His}$ is overexpressed in cells. Overall, the heatmap colour of unsupplemented cells differs from wildtype cells but is restored to levels resembling the wildtype expression profiles (Supplementary Figure S8G), indicating a major rescue of the proteome by $tRNA^{His}$ supplementation in cells the depend on CMT-mutant HARS for growth.

$tRNA^{His}$ supplementation rescues mistranslation and stabilizes HARS *in vivo* in V133F and Y330C

In a previous study, we showed that HARS mutants V155G and S356N caused mistranslation at histidine codons that was rescued by supplementation of histidine. In contrast, HARS mutants V133F and Y330C show a clear growth phenotype that is not remedied, and may even be exacerbated, by histidine supplementation (21). Here, we found that $tRNA^{His}$ alleviates the growth phenotype caused by HARS V133F and Y330C. We next tested if mistranslation can also be rescued by $tRNA^{His}$ supplementation. Using mass spectrometry, we found a 1.8-fold reduction in mistranslation events detected in cells expressing wildtype HARS and $tRNA^{His}$ compared to cells expressing wildtype HARS alone. Thirteen uniquely mistranslated peptides being identified in wildtype HARS expressing cells (Figure 8A), compared to 10 in supplemented cells. In these wildtype human HARS expressing cells supplemented with $tRNA^{His}$, two mistranslation to glutamine and eight to tyrosine incorporations at histidine codons were observed. (Figure 8E, Supplementary Figure S11). In cells expressing wildtype HARS, some mistranslated peptides were no longer observable after $tRNA^{His}$ supplementation (Figure 8B). The remaining mistranslated peptides did not show altered abundance between wildtype HARS supplemented and unsupplemented cells, as quantified by the area of the mistranslated peptide, which remains stable for most peptides in wildtype HARS expressing cells (Figure 8B). The data indicate that translation fidelity is restored, while the basal level of background mistranslation remains (19).

As described earlier, mistranslation in Y330C and V133F exceeds the basal mistranslation of wildtype HARS expressing cells by about 2-fold (Figure 8A). Upon supplementation with $tRNA^{His}$, mistranslation in both variants was decreased to wildtype basal levels. In V133F, we observed a significant 2.9-fold reduction in mistranslation events, with only 17 identified unique mistranslated peptides. Of these peptides, histidine codons were mistranslated to glutamine in seven peptides and to tyrosine in eight peptides (Figure 8E, I,J). Background level mis-incorporation of histidine at glutamic acid codons was still observed at similar levels following $tRNA^{His}$ supplementation (Supplementary Figure S12). While we already observed a significant decrease in the number of mistranslated peptides, the remaining mistranslated peptides were also reduced in abundance. By using the area under the isotopic peak of the mistranslated relative to the properly translated peptide, we found that following $tRNA^{His}$ supplementation

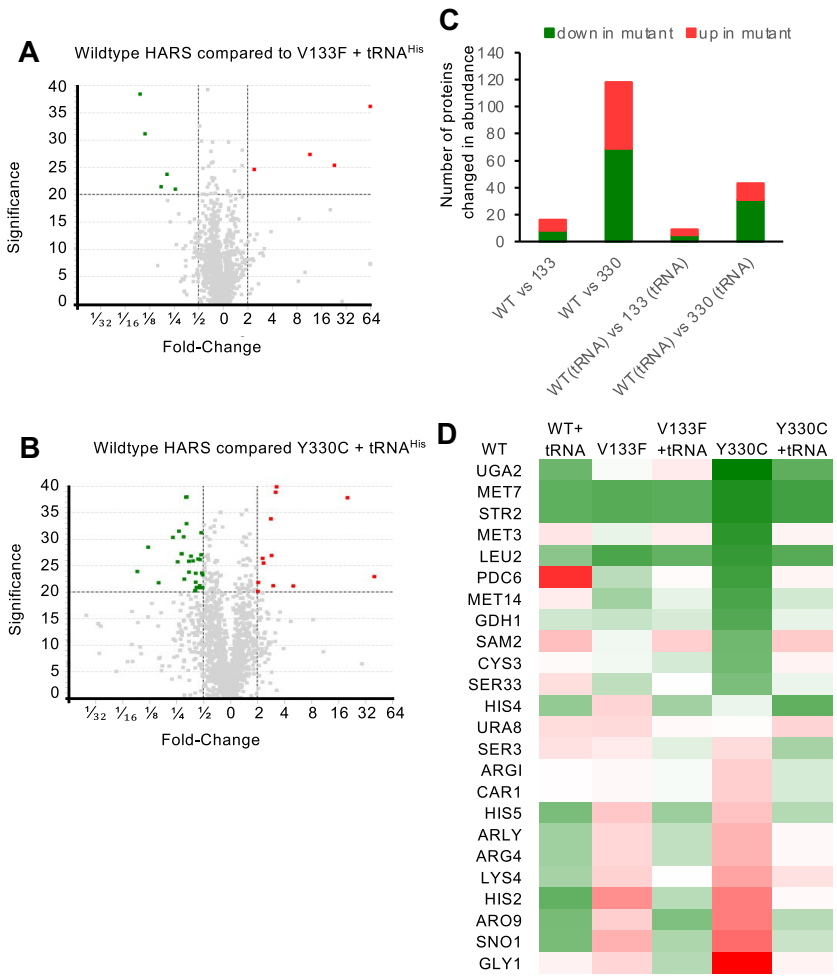

Figure 7. tRNA^{His} supplementation reduces proteome disturbances in HARS V133F and Y330C expressing cells. Volcano plots of differentially expressed proteins identified by label-free quantitative proteomic analysis between wildtype HARS and (**A**) V133F or (**B**) Y330C HARS following tRNA^{His} supplementation of all strains with upregulated proteins identified in red and downregulated proteins in green. (**C**) Number of proteins significantly changed in abundance by at least 2-fold, as identified by label-free quantification, between wildtype HARS and V133F or Y330C HARS, before and after tRNA^{His} supplementation. (**D**) Heat map of proteins with a role in amino acid metabolism that are up (red) and downregulated (green) compared to wildtype HARS with and without tRNA supplementation.

(Figure 8C) the abundance or level of mistranslated peptides was 10–20% of that in V133F cells lacking human tRNA^{His}.

Similar patterns were observed in Y330C following tRNA^{His} supplementation. Total mistranslation events were significantly reduced 3-fold (Figure 8A). We observed 20 uniquely mistranslated peptides, with seven and eight instances of glutamine and tyrosine incorporation at histidine codons, respectively (Figure 8E, Supplementary Figure S11). Similar background levels of histidine mis-incorporation at glutamic acid codons persisted following tRNA^{His} supplementation (Figure 8E, Supplementary Figure S12). As before, we observed a drastic decrease in the area under the isotopic peak for mistranslated relative to wildtype peptides following tRNA^{His} supplementation (Figure 8D).

To assess the impact of tRNA supplementation on HARS stability *in vivo*, we next compared soluble and insoluble proteins and whole cell lysates using a sedimentation assay. Following separation of whole lysates into soluble and insoluble fractions, we probed the samples with anti-GFP to identify HARS-YFP that is either soluble or insoluble, which can be indicative of HARS stability in yeast cells. Interestingly, HARS V133F and Y330C were significantly enriched in the insoluble protein fraction when compared to wildtype by 7.7- and 1.6-fold, respectively (Figure 8F,H, Supplementary Figure S13A-C), indicating mutant HARS aggregation in yeast. Following tRNA supplementation, mutant HARS solubility was restored to wildtype levels with no significant difference from the wildtype (Figure 8G,H, Supplementary Figure S13D,E,F). These data demonstrate that human tRNA^{His} supplementation effectively rescues mistranslation and HARS protein stability in cells caused by CMT-variants V133F and Y330C in human HARS.

Discussion

Several disease-causing mutations in HARS have been reported to date. The disease causing mechanisms vary from loss of function due to decreased thermal stability for the Usher syndrome associated Y454S mutation (16,21) to mutation induced conformational changes (39), loss of aminoacylation mutations (25,40) and impaired dimerization (41). We recently described a novel disease-causing mechanism for HARS mutations, where toxic HARS V155G and S356N gain-of-function mutations lead to mistranslation of histidine codons

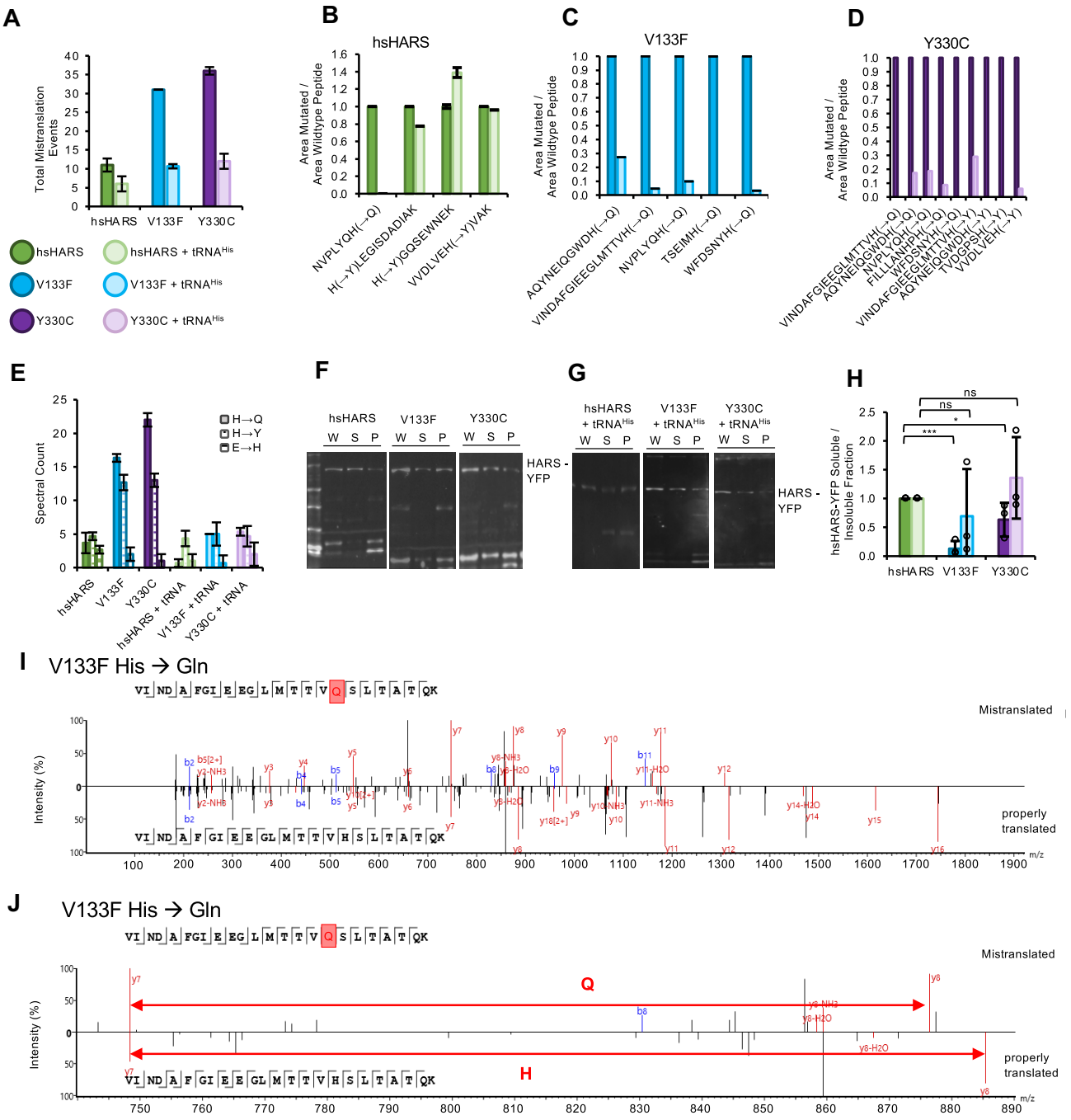

Figure 8. tRNA^{His} supplementation alleviates mistranslation in V133F and Y330C expressing yeast. (**A**) Total spectral counts of mistranslation events in whole proteome samples from humanized HARS WT, V133F and Y330C yeast. Error bars show one standard deviation of the mean. Quantification of the area under the isotopic of the of mistranslated peptide relative to the wildtype peptide normalized to the unsupplemented sample fraction of each peptide for (**B**) hsHARS, (**C**) V133F and (**D**)Y330C. (**E**) Mistranslation counts separated by type of mistranslation in untreated and tRNA-supplemented cells. Western blots for YFP-HARS of whole cell lysates from (**F**) unsupplemented and (**G**) tRNA^{His} supplemented yeast samples were separated into total [W], soluble [S] and insoluble [P] protein fractions, separated on a 12% SDS-denaturing polyacrylamide gel then transferred to PVDF membranes and blotted with anti-GFP. Ratios of the soluble to insoluble fraction were (**H**) quantified with normalization to the wildtype sample before and after tRNA^{His} supplementation; one standard deviation shown by error bars. Mirror plots of (**I**) HARS V133F with the difference in Y ions highlighted for (**J**) glutamine mis-incorporation at a histidine codons.

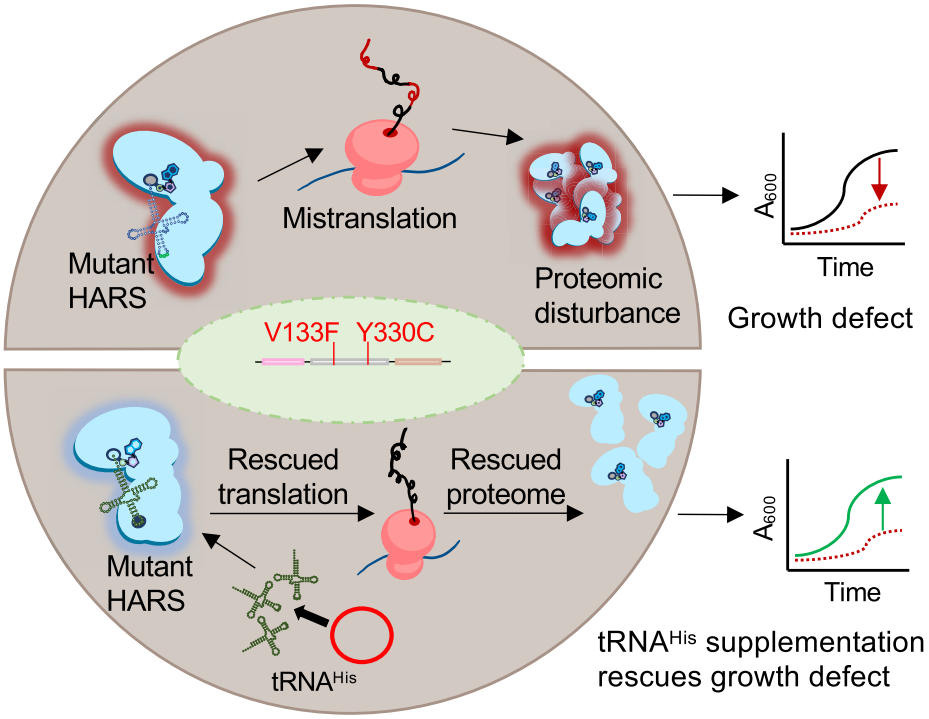

Figure 9. tRNA^{His} supplementation rescues disease-causing CMT mutants in a yeast model. (**A**) Reduced HARS stability in HARS V133F and Y330C lead to mistranslation, the accumulation of insoluble HARS and changes to the proteome focused on amino acid metabolism in a humanized yeast model of CMT. Supplementation with human tRNA^{His} restores V133F CMT-HARS protein structure and alleviates mistranslation in both V133F and Y330C as well as insoluble HARS accumulation in cells.

to non-histidine amino acids, causing widespread accumulation of insoluble proteins (21). For these mutants, alternate amino acids, such as glutamine, were detected in place of histidine, indicating impaired amino acid selectivity by the mutant HARS. For both mutants, the phenotype in humanized yeast models was rescued by histidine supplementation (21).

Here, we identified a second mistranslation phenotype in two other CMT-HARS mutants V133F and Y330C (Figure 9). HARS V133F and Y330C were previously characterized as disease-causing mutations in CMT patients. HARS V133F leads to reduced aminoacylation activity in patient derived cells (42) and has an autosomal dominant inheritance pattern (43), and HARS Y330C leads to a dominant negative phenotype in zebrafish and was found to reduce aminoacylation and induce the integrated stress response (ISR) (44). We recently showed that both mutants lead to a reduced growth phenotype in yeast, which cannot be rescued by histidine supplementation, and indeed increased histidine concentrations caused insoluble protein accumulation (21). A recent breakthrough demonstrated that tRNAs can be utilized as a therapeutic, where supplementation of wildtype cognate tRNAs rescued peripheral neuropathy, protein synthesis and the activation of the ISR in Drosophila and mouse CMT models (31). In this case, the overexpression of tRNA^{Gly} is thought to compensate for the increased affinity of a mutant GARS protein to its cognate tRNA, resulting in tRNA^{Gly} sequestration (31), providing a first example of the potential therapeutic of cognate or wildtype tRNA.

In our study, supplementation of wildtype tRNA^{His} rescued a humanized yeast growth phenotype, yet the underlying disease-causing phenotype is distinct from other CMT-HARS mutants (Figure 9). HARS Y330C does not impact protein stability yet causes mistranslation in yeast leading to a significant growth phenotype and proteomic disturbance that can be restored by tRNA^{His} supplementation. As the mistranslation of glutamic acid to histidine is evident in wildtype HARS expressing cells and remains stable after tRNA^{His} supplementation, it is unlikely that the mutant HARS is recognizing a non-cognate tRNA, but rather due to background levels of mistranslation that occurs in all cells as reviewed previously (19,45–46). HARS V133F shows a dual phenotype of mistranslation and reduced protein stability, which leads to reduced growth in yeast that is exacerbated by histidine supplementation causing insoluble protein aggregation (21). Recombinant V133F thermal lability can be rescued by the addition of a tRNA^{His}, and tRNA supplementation rescues the growth defect in yeast to wildtype levels, indicating that the tRNA^{His} restores HARS V133F function, while also preventing mistranslation. It is likely that tRNA^{His} leads to restoration of protein stability returning the structural integrity and amino acid specificity of HARS to wildtype levels.

Given that Y330C caused a notable alteration in the cellular proteome, it is likely that mistranslation in this strain exceeds tolerable levels, indicating that Y330C causes a toxic gain of function. In Y330C yeast, amino acid metabolism is one of the most effected metabolic pathways. Altered expression of amino acid metabolic proteins has previously been associated with the cellular stress response and activation of GCN4 (47), though no activation of the ISR protein GCN4 was observed in our proteomic analysis. Indeed no GCN4 peptides were detected under any conditions (Supplemental File S1), and we previously did not observe an activation of the ISR by eIF2a

phosphorylation (21). Additionally, HSP70 upregulation is associated with mistranslation in cells (48), and HAC1, SSA4 and HSP104 are activated in the presence of uncharged tRNAs (47,48). While HAC1 was undetectable, we found only HSP70 significantly upregulated in both yeast strains, with no changes in SSA4 and HSP104 in V133F cells, and a significant downregulation of SSA4 and HSP104 in Y330C cells, indicating partial activation of the unfolded protein response. Activation of the unfolded protein response and upregulation of heat shock proteins was previously observed in response to mistranslation and altered RNA processing pathways (49,50). It is likely yeast differentially regulate chaperones and amino acid biosynthesis, especially upregulated histidine biosynthesis, and ribosome biogenesis, in an attempt to rescue halted translation. Excitingly, our data shows that for HARS Y330C and V133F, all measured phenotypes were rescued by $tRNA^{His}$ supplementation, restoring translation fidelity, growth and proteome composition to wildtype levels.

Conclusion

We presented the first example where wildtype tRNA supplementation can rescue a disease phenotype caused by mistranslation. Applications of tRNA therapeutics have gained traction in both academic and industry-led research teams (51), and may soon move into clinical applications. While nonsense suppressor tRNAs (52–56) show great promise in restoring protein function from disease-causing alleles with premature stop codons, we and others (31) show that wildtype tRNA expression can rescue disease phenotypes caused by mutations in aaRSs and give rise to new disease-specific treatments for CMT and many rare genetic diseases caused by mutations in aaRSs.

The mass spectrometry proteomics data have been deposited to the ProteomeXchange Consortium via the PRIDE partner repository with the dataset identifier PXD050340.

Supplementary data

Supplementary Data are available at NAR Online.

Acknowledgements

We thank Vicky Siu, Tony Rupar, Patrick Lajoie and Martin Duennwald for advice and critical discussion.

Funding

Natural Sciences and Engineering Research Council of Canada [04776 to I.U.H; 04282 to P.O.]; Canada Research Chairs [232341 to P.O.]; Canadian Institutes of Health Research [165985 to P.O.; 185961 to I.U.H]; Ontario Ministry of Research and Innovation [ER-18-14-183 to I.U.H]; Huntington Society of Canada Endowed Research Chair [to P.O.]; and a Rare Disease Models and Mechanism Grant [to I.U.H] and a Canada Graduate Scholarship (Masters program) [to S.W.].

Conflict of interest statement

None declared.

References

1. Morena,J., Gupta,A. and Hoyle,J.C. (2019) Charcot-Marie-Tooth: from molecules to therapy. *Int. J. Mol. Sci.*, **20**, 3419.
2. Theadom,A., Roxburgh,R., Macaulay,E., O'Grady,G., Burns,J., Parmar,P., Jones,K. and Rodrigues,M. (2019) Prevalence of Charcot-Marie-Tooth disease across the lifespan: a population-based epidemiological study. *BMJ Open*, **9**, e029240.
3. Antonellis,A., Ellsworth,R.E., Sambuughin,N., Puls,I., Abel,A., Lee-Lin,S.Q., Jordanova,A., Kremensky,I., Christodoulou,K., Middleton,L.T., *et al.* (2003) Glycyl tRNA synthetase mutations in Charcot-Marie-Tooth disease type 2D and distal spinal muscular atrophy type V. *Am. J. Hum. Genet.*, **72**, 1293–1299.
4. Jordanova,A., Irobi,J., Thomas,F.P., Van Dijck,P., Meerschaert,K., Dewil,M., Dierick,I., Jacobs,A., De Vriendt,E., Guergueltcheva,V., *et al.* (2006) Disrupted function and axonal distribution of mutant tyrosyl-tRNA synthetase in dominant intermediate Charcot-Marie-Tooth neuropathy. *Nat. Genet.*, **38**, 197–202.
5. Latour,P., Thauvin-Robinet,C., Baudelet-Mery,C., Soichot,P., Cusin,V., Faivre,L., Locatelli,M.C., Mayencon,M., Sarcey,A., Broussolle,E., *et al.* (2010) A major determinant for binding and aminoacylation of tRNA (Ala) in cytoplasmic Alanyl-tRNA synthetase is mutated in dominant axonal Charcot-Marie-Tooth disease. *Am. J. Hum. Genet.*, **86**, 77–82.
6. Safka Brozkova,D., Deconinck,T., Griffin,L.B., Ferbert,A., Haberlova,J., Mazanec,R., Lassuthova,P., Roth,C., Pilunthanakul,T., Rautenstrauss,B., *et al.* (2015) Loss of function mutations in HARS cause a spectrum of inherited peripheral neuropathies. *Brain*, **138**, 2161–2172.
7. Gonzalez,M., McLaughlin,H., Houlden,H., Guo,M., Yo-Tsen,L., Hadjivassilious,M., Speziani,F., Yang,X.L., Antonellis,A., Reilly,M.M., *et al.* (2013) Exome sequencing identifies a significant variant in methionyl-tRNA synthetase (MARS) in a family with late-onset CMT2. *J. Neurol. Neurosurg. Psychiatry*, **84**, 1247–1249.
8. Tsai,P.C., Soong,B.W., Mademan,I., Huang,Y.H., Liu,C.R., Hsiao,C.T., Wu,H.T., Liu,T.T., Liu,Y.T., Tseng,Y.T., *et al.* (2017) A recurrent WARS mutation is a novel cause of autosomal dominant distal hereditary motor neuropathy. *Brain*, **140**, 1252–1266.
9. Wilhelm,S.D.P., Kenana,R., Qiu,Y., O'Donoghue,P. and Heinemann,I.U. (2023) Towards a cure for HARS Disease. *Genes (Basel)*, **14**, 254.
10. Meyer-Schuman,R. and Antonellis,A. (2017) Emerging mechanisms of aminoacyl-tRNA synthetase mutations in recessive and dominant human disease. *Hum. Mol. Genet.*, **26**, R114–R127.
11. Freist,W., Verhey,J.F., Ruhlmann,A., Gauss,D.H. and Arnez,J.G. (2005) Histidyl-tRNA Synthetase. *J. Biol. Chem.*, **380**, 623–646.
12. Chen,A.W., Jayasinghe,M.I., Chung,C.Z., Rao,B.S., Kenana,R., Heinemann,I.U. and Jackman,J.E. (2019) The role of 3' to 5' reverse RNA polymerization in tRNA fidelity and repair. *Genes (Basel)*, **10**, 250.
13. Heinemann,I.U., Nakamura,A., O'Donoghue,P., Eiler,D. and Soll,D. (2012) tRNAHis-guanylyltransferase establishes tRNAHis identity. *Nucleic Acids Res.*, **40**, 333–344.
14. Howard,O.M., Dong,H.F., Yang,D., Raben,N., Nagaraju,K., Rosen,A., Casciola-Rosen,L., Hartlein,M., Kron,M., Yang,D., *et al.* (2002) Histidyl-tRNA synthetase and asparaginyl-tRNA synthetase, autoantigens in myositis, activate chemokine receptors on T lymphocytes and immature dendritic cells. *J. Exp. Med.*, **196**, 781–791.
15. Mathews,M.B. and Bernstein,R.M. (1983) Myositis autoantibody inhibits histidyl-tRNA synthetase: a model for autoimmunity. *Nature*, **304**, 177–179.
16. Abbott,J.A., Guth,E., Kim,C., Regan,C., Siu,V.M., Rupar,C.A., Demeler,B., Francklyn,C.S. and Robey-Bond,S.M. (2017) The Usher Syndrome Type IIIB Histidyl-tRNA synthetase mutation confers temperature sensitivity. *Biochemistry*, **56**, 3619–3631.
17. Puffenberger,E.G., Jinks,R.N., Sougnez,C., Cibulskis,K., Willert,R.A., Achilly,N.P., Cassidy,R.P., Fiorentini,C.J., Heiken,K.F., Lawrence,J.J., *et al.* (2012) Genetic mapping and

exome sequencing identify variants associated with five novel diseases. *PLoS One*, **7**, e28936.
18. Kwon,N.H., Fox,P.L. and Kim,S. (2019) Aminoacyl-tRNA synthetases as therapeutic targets. *Natl. Rev. Drug Discov.*, **18**, 629–650.
19. Lant,J.T., Berg,M.D., Heinemann,I.U., Brandl,C.J. and O'Donoghue,P. (2019) Pathways to disease from natural variations in human cytoplasmic tRNAs. *J. Biol. Chem.*, **294**, 5294–5308.
20. Rozik,P., Szabla,R., Lant,J.T., Kiri,R., Wright,D.E., Junop,M. and O'Donoghue,P. (2022) A novel fluorescent reporter sensitive to serine mis-incorporation. *RNA Biol.*, **19**, 221–233.
21. Qiu,Y., Kenana,R., Beharry,A., Wilhelm,S.D.P., Hsu,S.Y., Siu,V.M., Duennwald,M. and Heinemann,I.U. (2023) Histidine supplementation can escalate or rescue HARS deficiency in a Charcot-Marie-Tooth disease model. *Hum. Mol. Genet.*, **32**, 810–824.
22. Mendonsa,S., von Kuegelgen,N., Bujanic,L. and Chekulaeva,M. (2021) Charcot-Marie-Tooth mutation in glycyl-tRNA synthetase stalls ribosomes in a pre-accommodation state and activates integrated stress response. *Nucleic Acids Res.*, **49**, 10007–10017.
23. Niehues,S., Bussmann,J., Steffes,G., Erdmann,I., Kohrer,C., Sun,L., Wagner,M., Schafer,K., Wang,G., Koerdt,S.N., *et al.* (2015) Impaired protein translation in Drosophila models for Charcot-Marie-Tooth neuropathy caused by mutant tRNA synthetases. *Nat. Commun.*, **6**, 7520.
24. Ward,C., Beharry,A., Tennakoon,R., Rozik,P., Wilhelm,S.D.P., Heinemann,I.U. and O'Donoghue,P. (2024) Mechanisms and delivery of tRNA therapeutics. *Chem. Rev.*, **124**, 7976–8008.
25. Abbott,J.A., Livingston,N.M., Egri,S.B., Guth,E. and Francklyn,C.S. (2017) Characterization of aminoacyl-tRNA synthetase stability and substrate interaction by differential scanning fluorimetry. *Methods*, **113**, 64–71.
26. Jin,D., Wek,S.A., Cordova,R.A., Wek,R.C., Lacombe,D., Michaud,V. and Musier-Forsyth,K. (2023) Aminoacylation-defective bi-allelic mutations in human EPRS1 associated with psychomotor developmental delay, epilepsy, and deafness. *Clin. Genet.*, **103**, 358–363.
27. Whitmore,L. and Wallace,B.A. (2004) DICHROWEB, an online server for protein secondary structure analyses from circular dichroism spectroscopic data. *Nucleic Acids Res.*, **32**, W668–W673.
28. Sreerama,N. and Woody,R.W. (2000) Estimation of protein secondary structure from circular dichroism spectra: comparison of CONTIN, SELCON, and CDSSTR methods with an expanded reference set. *Anal. Biochem.*, **287**, 252–260.
29. Varshney,U., Lee,C.P. and RajBhandary,U.L. (1991) Direct analysis of aminoacylation levels of tRNAs in vivo. Application to studying recognition of Escherichia coli initiator tRNA mutants by glutaminyl-tRNA synthetase. *J. Biol. Chem.*, **266**, 24712–24718.
30. Shiber,A., Breuer,W., Brandeis,M. and Ravid,T. (2013) Ubiquitin conjugation triggers misfolded protein sequestration into quality control foci when Hsp70 chaperone levels are limiting. *Mol. Biol. Cell*, **24**, 2076–2087.
31. Zuko,A., Mallik,M., Thompson,R., Spaulding,E.L., Wienand,A.R., Been,M., Tadenev,A.L.D., van Bakel,N., Sijlmans,C., Santos,L.A., *et al.* (2021) tRNA overexpression rescues peripheral neuropathy caused by mutations in tRNA synthetase. *Science*, **373**, 1161–1166.
32. Rosen,A.E., Brooks,B.S., Guth,E., Francklyn,C.S. and Musier-Forsyth,K. (2006) Evolutionary conservation of a functionally important backbone phosphate group critical for aminoacylation of histidine tRNAs. *RNA*, **12**, 1315–1322.
33. Szklarczyk,D., Kirsch,R., Koutrouli,M., Nastou,K., Mehryary,F., Hachilif,R., Gable,A.L., Fang,T., Doncheva,N.T., Pyysalo,S., *et al.* (2023) The STRING database in 2023: protein-protein association networks and functional enrichment analyses for any sequenced genome of interest. *Nucleic Acids Res.*, **51**, D638–D646.
34. Harashima,S., Sidhu,R.S., Toh-e,A. and Oshima,Y. (1981) Cloning of the HIS5 gene of *Saccharomyces cerevisiae* by yeast transformation. *Gene*, **16**, 335–341.
35. Keesey,J.K. Jr., Bigelis,R. and Fink,G.R. (1979) The product of the his4 gene cluster in *Saccharomyces cerevisiae*. A trifunctional polypeptide. *J. Biol. Chem.*, **254**, 7427–7433.
36. Chan,P.P. and Lowe,T.M. (2016) GtRNAdb 2.0: an expanded database of transfer RNA genes identified in complete and draft genomes. *Nucleic Acids Res.*, **44**, D184–D189.
37. Chan,P.P. and Lowe,T.M. (2009) GtRNAdb: a database of transfer RNA genes detected in genomic sequence. *Nucleic Acids Res.*, **37**, D93–D97.
38. Natsoulis,G., Hilger,F. and Fink,G.R. (1986) The HTS1 gene encodes both the cytoplasmic and mitochondrial histidine tRNA synthetases of S. cerevisiae. *Cell*, **46**, 235–243.
39. Blocquel,D., Sun,L., Matuszek,Z., Li,S., Weber,T., Kuhle,B., Kooi,G., Wei,N., Baets,J., Pan,T., *et al.* (2019) CMT disease severity correlates with mutation-induced open conformation of histidyl-tRNA synthetase, not aminoacylation loss, in patient cells. *Proc. Natl. Acad. Sci. USA*, **116**, 19440–19448.
40. Vester,A., Velez-Ruiz,G., McLaughlin,H.M., Program,N.C.S., Lupski,J.R., Talbot,K., Vance,J.M., Zuchner,S., Roda,R.H., Fischbeck,K.H., *et al.* (2013) A loss-of-function variant in the human histidyl-tRNA synthetase (HARS) gene is neurotoxic in vivo. *Hum. Mutat.*, **34**, 191–199.
41. Wilhelm,S.D.P., Moresco,A.A., Rivero,A.D., Siu,V.M. and Heinemann,I.U. (2024) Characterization of a novel heterozygous variant in the histidyl-tRNA synthetase gene associated with Charcot-Marie-Tooth disease type 2W. *IUBMB Life*, https://doi.org/10.1002/iub.2918.
42. Royer-Bertrand,B., Tsouni,P., Mullen,P., Campos Xavier,B., Mittaz Crettol,L., Lobrinus,A.J., Ghika,J., Baumgartner,M.R., Rivolta,C., Superti-Furga,A., *et al.* (2019) Peripheral neuropathy and cognitive impairment associated with a novel monoallelic HARS variant. *Ann. Clin. Transl. Neurol.*, **6**, 1072–1080.
43. Lahoz Alonso,R., Sienes Bailo,P., Capablo Liesa,J.L., Alvarez de Andres,S., Bancalero Flores,J.L. and Izquierdo Alvarez,S. (2020) A variant of the gene HARS detected in the clinical exome: etiology of a peripheral neuropathy undiagnosed for 20 years. *Adv. Lab Med.*, **1**, 20200033.
44. Mullen,P., Abbott,J.A., Wellman,T., Aktar,M., Fjeld,C., Demeler,B., Ebert,A.M. and Francklyn,C.S. (2021) Neuropathy-associated histidyl-tRNA synthetase variants attenuate protein synthesis in vitro and disrupt axon outgrowth in developing zebrafish. *FEBS J.*, **288**, 142–159.
45. Schwartz,M.H. and Pan,T. (2017) Function and origin of mistranslation in distinct cellular contexts. *Crit. Rev. Biochem. Mol. Biol.*, **52**, 205–219.
46. Raikwar,S.P. and Zavazava,N. (2009) Real-time non-invasive imaging of ES cell-derived insulin producing cells. *Methods Mol. Biol.*, **590**, 317–334.
47. Mohler,K., Mann,R., Bullwinkle,T.J., Hopkins,K., Hwang,L., Reynolds,N.M., Gassaway,B., Aerni,H.R., Rinehart,J., Polymenis,M., *et al.* (2017) Editing of misaminoacylated tRNA controls the sensitivity of amino acid stress responses in *Saccharomyces cerevisiae*. *Nucleic Acids Res.*, **45**, 3985–3996.
48. Grant,C.M., Firoozan,M. and Tuite,M.F. (1989) Mistranslation induces the heat-shock response in the yeast *Saccharomyces cerevisiae*. *Mol. Microbiol.*, **3**, 215–220.
49. Chung,C.Z., Jaramillo,J.E., Ellis,M.J., Bour,D.Y.N., Seidl,L.E., Jo,D.H.S., Turk,M.A., Mann,M.R., Bi,Y., Haniford,D.B., *et al.* (2019) RNA surveillance by uridylation-dependent RNA decay in *Schizosaccharomyces pombe*. *Nucleic Acids Res.*, **47**, 3045–3057.
50. Hoffman,K.S., Berg,M.D., Shilton,B.H., Brandl,C.J. and O'Donoghue,P. (2017) Genetic selection for mistranslation rescues a defective co-chaperone in yeast. *Nucleic Acids Res.*, **45**, 3407–3421.
51. Dolgin,E. (2022) tRNA therapeutics burst onto startup scene. *Nat. Biotechnol.*, **40**, 283–286.

52. Hasan,F., Lant,J.T. and O'Donoghue,P. (2023) Perseverance of protein homeostasis despite mistranslation of glycine codons with alanine. *Philos. Trans. R. Soc. Lond. B Biol. Sci.*, **378**, 20220029.
53. Lant,J.T., Hasan,F., Briggs,J., Heinemann,I.U. and O'Donoghue,P. (2023) Genetic Interaction of tRNA-Dependent Mistranslation with Fused in Sarcoma Protein Aggregates. *Genes (Basel)*, **14**, 518.
54. Albers,S., Allen,E.C., Bharti,N., Davyt,M., Joshi,D., Perez-Garcia,C.G., Santos,L., Mukthavaram,R., Delgado-Toscano,M.A., Molina,B., *et al.* (2023) Engineered tRNAs suppress nonsense mutations in cells and in vivo. *Nature*, **618**, 842–848.
55. Ko,W., Porter,J.J., Sipple,M.T., Edwards,K.M. and Lueck,J.D. (2022) Efficient suppression of endogenous CFTR nonsense mutations using anticodon-engineered transfer RNAs. *Mol. Ther. Nucleic Acids*, **28**, 685–701.
56. Wang,J., Zhang,Y., Mendonca,C.A., Yukselen,O., Muneeruddin,K., Ren,L., Liang,J., Zhou,C., Xie,J., Li,J., *et al.* (2022) AAV-delivered suppressor tRNA overcomes a nonsense mutation in mice. *Nature*, **604**, 343–348.

Received: March 15, 2024. **Revised:** September 13, 2024. **Editorial Decision:** October 10, 2024. **Accepted:** October 16, 2024